

RESEARCH ARTICLE

10.1002/2016WR019712

Special Section:

Concentration-discharge Relationships in the Critical Zone

Key Points:

- Probing Na and Si fluxes across different timescales reveals geochemical processes controlling C-Q relationships
- Chemostatic behavior of base cations and DIC explained by mixing of water displaced from residence in various hydrogeologic reservoirs
- DOC, Al, and Ge/Si increase with discharge from organic matter complexation and colloidal transport during soil flushing

Correspondence to:

J. McIntosh,
mcintosh@hwr.arizona.edu

Citation:

McIntosh, J. C., et al. (2017), Geochemical evolution of the Critical Zone across variable time scales informs concentration-discharge relationships: Jemez River Basin Critical Zone Observatory, *Water Resour. Res.*, 53, 4169–4196, doi:10.1002/2016WR019712.









Received 29 AUG 2016

Accepted 25 APR 2017

Accepted article online 2 MAY 2017

Published online 23 MAY 2017

Geochemical evolution of the Critical Zone across variable time scales informs concentration-discharge relationships: Jemez River Basin Critical Zone Observatory

Jennifer C. McIntosh¹ , Courtney Schaumberg¹, Julia Perdrial² , Adrian Harpold³ , Angélica Vázquez-Ortega⁴, Craig Rasmussen⁵ , David Vinson⁶, Xavier Zapata-Rios¹ , Paul D. Brooks⁷ , Thomas Meixner¹, Jon Pelletier⁸, Louis Derry⁹ , and Jon Chorover⁵ 

¹Department of Hydrology and Atmospheric Sciences, University of Arizona, Tucson, Arizona, USA, ²Department of Geology, University of Vermont, Burlington, Vermont, USA, ³Department of Natural Resources and Environmental Science, University of Nevada, Reno, Nevada, USA, ⁴Department of Civil and Environmental Engineering and Earth Sciences, University of Notre Dame, South Bend, Indiana, USA, ⁵Department of Soil, Water and Environmental Science, University of Arizona, Tucson, Arizona, USA, ⁶Department of Geography and Earth Sciences, University of North Carolina, Charlotte, North Carolina, USA, ⁷Department of Geology and Geophysics, University of Utah, Salt Lake City, Utah, USA, ⁸Department of Geosciences, University of Arizona, Tucson, Arizona, USA, ⁹Department of Earth and Atmospheric Sciences, Cornell University, Ithaca, New York, USA

Abstract This study investigates the influence of water, carbon, and energy fluxes on solute production and transport through the Jemez Critical Zone (CZ) and impacts on C-Q relationships over variable spatial and temporal scales. Chemical depletion-enrichment profiles of soils, combined with regolith thickness and groundwater data indicate the importance to stream hydrochemistry of incongruent dissolution of silicate minerals during deep bedrock weathering, which is primarily limited by water fluxes, in this highly fractured, young volcanic terrain. Under high flow conditions (e.g., spring snowmelt), wetting of soil and regolith surfaces and presence of organic acids promote mineral dissolution and provide a constant supply of base cations, Si, and DIC to soil water and groundwater. Mixing of waters from different hydrochemical reservoirs in the near stream environment during “wet” periods leads to the chemostatic behavior of DIC, base cations, and Si in stream flow. Metals transported by organic matter complexation (i.e., Ge, Al) and/or colloids (i.e., Al) during periods of soil saturation and lateral connectivity to the stream display a positive relationship with Q. Variable Si-Q relationships, under all but the highest flow conditions, can be explained by nonconservative transport and precipitation of clay minerals, which influences long versus short-term Si weathering fluxes. By combining measurements of the CZ obtained across different spatial and temporal scales, we were able to constrain weathering processes in different hydrological reservoirs that may be flushed to the stream during hydrologic events, thereby informing C-Q relationships.

1. Introduction

The Critical Zone (CZ), the thin, living skin of the earth, from the top of canopies down to saturated bedrock, provides vital environmental and human services, such as water storage, nutrient cycling, water purification, and climate regulation [Field et al., 2015]. The heterogeneous structure of the CZ, such as distribution of clays and pore networks, can develop over long (geologic) timescales in response to variations in lithology [e.g., Brantley et al., 2017], as well as water, energy, and carbon availability [Chorover et al., 2011], as a function of landscape position and/or aspect [e.g., Pelletier et al., 2013], or short (episodic) timescales due to disturbance, such as fire [Orem and Pelletier, 2016] and land use change [Gallo et al., 2012, 2013; Hall et al., 2016]. This heterogeneity controls the flux of water, gases, and solutes through the CZ, and alters water storage, transit times, and flow paths. Understanding the coupling of CZ development over long and short timescales, and between deep and shallow weathering processes, is one of the grand challenges for CZ science [Brantley et al., 2007; Chorover et al., 2011; Goddérís and Brantley, 2013; Brooks et al., 2015].

Concentration-discharge (C-Q) relationships can provide useful insights into CZ structure and function on relatively short timescales, as the hydrochemical response of streams can vary with flow paths, transit times and fluxes, mineral weathering rates, and biogeochemical processing [Godsey et al., 2009; Maher, 2011;

Shanley et al., 2011]. For example, during storm events or spring snowmelt, flushing of near surface soils typically is associated with a hysteretic pattern in surface water organic carbon concentrations [Hornberger et al., 1994; Boyer et al., 1997; Hood et al., 2003; Bishop et al., 2004; Brooks and Lemon, 2007; Liu et al., 2008a, 2008b; Sebestyen et al., 2008; Biederman et al., 2016]. These patterns have been associated with transient water sources and flow paths that intersect surface soils characterized by higher organic carbon content and higher hydraulic conductivity than deeper, mineral soils [Hornberger et al., 1994; Chanut et al., 2002; Bishop et al., 2004; Hood et al., 2006; Brooks and Lemon, 2007; Biederman et al., 2016]. Metals, such as Al, Fe, and rare earth elements and yttrium (REY) can be cotransported with colloidal and dissolved organic carbon (DOC) [Sposito, 2008; Chorover, 2012; Vázquez-Ortega et al., 2015; Trostle et al., 2016], although they may not necessarily have the same origin [Burns et al., 2016].

When correlating base cations and Si concentrations (C) with stream discharge (Q), typically little change in C with increasing Q ("chemostatic behavior") or slight dilution effects (C decreases slightly with increasing Q) are observed if both water and solutes come from the same, well-mixed reservoir [Brooks et al., 2015; Hall et al., 2016]. Mechanisms for chemostasis have been postulated to derive from high chemical reaction rates relative to advective mass transport rates in catchment systems (i.e., high Damköhler numbers) [e.g., Johnson and DePaolo, 1994; Steefel and Maher, 2009; Maher, 2010; Maher and Chamberlain, 2014]. In contrast, solutes that exhibit a flushing response (e.g., DOC and associated metals; where C typically increases with increasing Q) often exhibit hysteresis in C-Q relationships where concentrations for a given discharge differ on the ascending versus descending limbs of the event hydrograph [Hornberger et al., 2001; Brooks et al., 2001; Trostle et al., 2016]. During flushing events, these hysteretic patterns often are positive, with higher concentrations on the ascending limb, but the timing and degree of activation of different flow paths or water sources also can result in negative hysteresis with higher concentrations on the descending limb [Evans and Davies, 1998; Chanut et al., 2002]. Even though these general patterns are commonly observed, the underlying causes of variability in C-Q relationships over variable timescales and drivers (e.g., water and energy inputs) remain an open question. An integrative approach that probes the entire CZ, including drivers of water and solute fluxes (e.g., climate), CZ structure (e.g., soil and regolith chemical composition), and hydrological response is needed to address these questions.

This study investigates the mechanisms controlling C-Q relationships over variable spatial and time scales in a montane, headwater catchment in the southwestern United States. The long-term evolution of the CZ, which controls distribution of solid phases contributing to modern solute generation, flow paths, and transit times, was investigated through chemical enrichment/depletion profiles of soils with different hydrologic fluxes and microclimates based on landscape position and aspect. Long-term Na and Si weathering rates of soils were then compared to short-term solute fluxes using soil water and stream water chemistry to describe the production and retention of solutes in the CZ over a range of timescales. The geochemical evolution of waters through the CZ was investigated to understand biogeochemical processes controlling solute chemistry in various hydrologic reservoirs that may be connected to the stream during hydrologic events. Stream water C-Q relationships and time-series data of solute chemistry and discharge provide insight into how weathering reactions, source water contributions, and flow paths to streams vary with climate. Understanding of the reservoirs and fluxes of water, carbon, and solutes through the CZ provides insights into the controlling factors of C-Q relationships, and informs coupling of CZ processes over variable spatial and time scales.

2. Methods

2.1. Study Area

This study is focused on a small (3.3 km²) headwater catchment (La Jara Creek, Figures 1 and 2), draining Redondo Peak (elevation: 2728–3432m) in a montane mixed conifer forest within the Valles Caldera National Preserve (VCNP) in the Jemez Mountains in northern New Mexico (Figure 1). The headwater catchment includes an instrumented subcatchment or zero-order basin (ZOB; 0.15 km², Figure 3a). The La Jara catchment is part of the Jemez River Basin-Critical Zone Observatory (JRB-CZO) [Chorover et al., 2011]. The Jemez Mountains are in the transition zone between the snow-dominated Rocky Mountains and the monsoon-dominated southwestern United States, resulting in a bimodal pattern of annual precipitation [Brooks and Vivoni, 2008]. The Quemazon Snow Telemetry (SNOTEL) station, located approximately 10 km

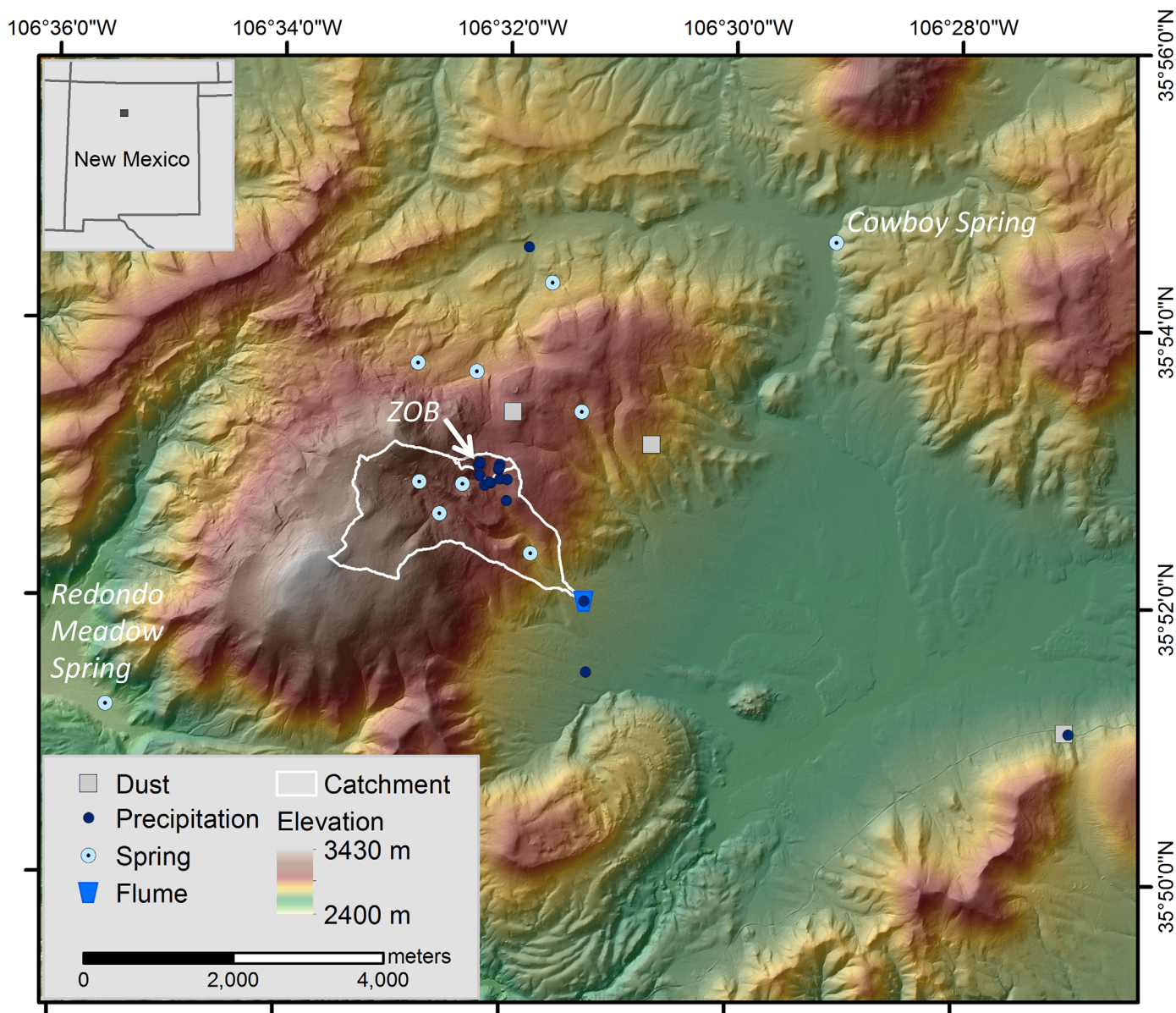


Figure 1. Location and topography of the La Jara Creek catchment (outlined in white), draining the southeastern side of Redondo Peak in the Valles Caldera National Preserve (VCNP), site of the Jemez River Basin Critical Zone Observatory (JRB-CZO), New Mexico. Sample locations are also indicated for precipitation (snow and rain) and dust collectors, springs, and La Jara creek stream water (flume at catchment outlet). The Mixed Conifer Zero Order Basin (ZOB), a focused JRB-CZO study site within the La Jara Creek catchment, is also outlined in white.

west and 100 m lower than the field site, has been in operation since 1981. Mean water year precipitation from 1981 to 2012 was 71 cm, of which 44% fell as snow. The remaining precipitation comes from summer monsoon rains [Molotch *et al.*, 2009; Broxton *et al.*, 2009]. Temperature ranges from -15°C (low) in the winter to 25°C (high) in the summer [Broxton *et al.*, 2009].

2.1.1. Geology

Redondo Peak, a resurgent volcanic dome in the center of the Valles Caldera, is primarily underlain by Quaternary aged rhyolitic volcanoclastics (<http://geoinfo.nmt.edu/publications/maps/geologic/ofgm/>) (Figure 2). The bedrock within the ZOB, on the southeastern side of Redondo Peak, is a complex mixture of highly fractured porphyritic rhyodacite, and partially welded, hydrothermally altered Bandelier Tuff (Figure 3b). The fine-grained rhyodacite is composed of albite, quartz, and alkali feldspar, while the Bandelier Tuff is composed of Ca-clinoptilolite, alkali feldspars, and cristobalite [Vázquez-Ortega *et al.*, 2016]. There is also an outcropping of sandstone that fell into the caldera after eruption and was incorporated with the volcanic

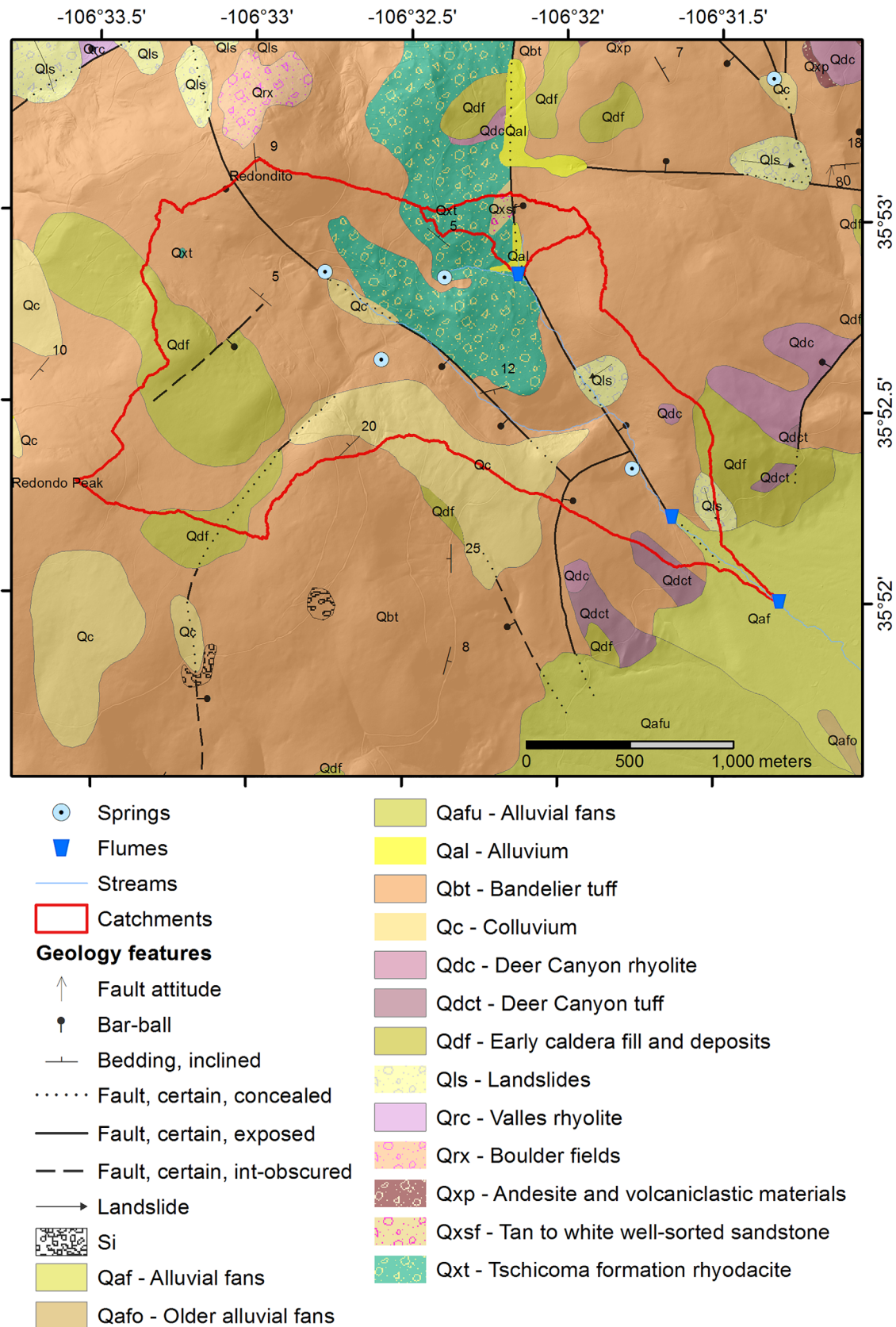


Figure 2. Bedrock geology map of La Jara catchment [Goff et al., 2005, 2006a, 2006b; Goff, 2009] indicating locations of springs and flumes sampled.

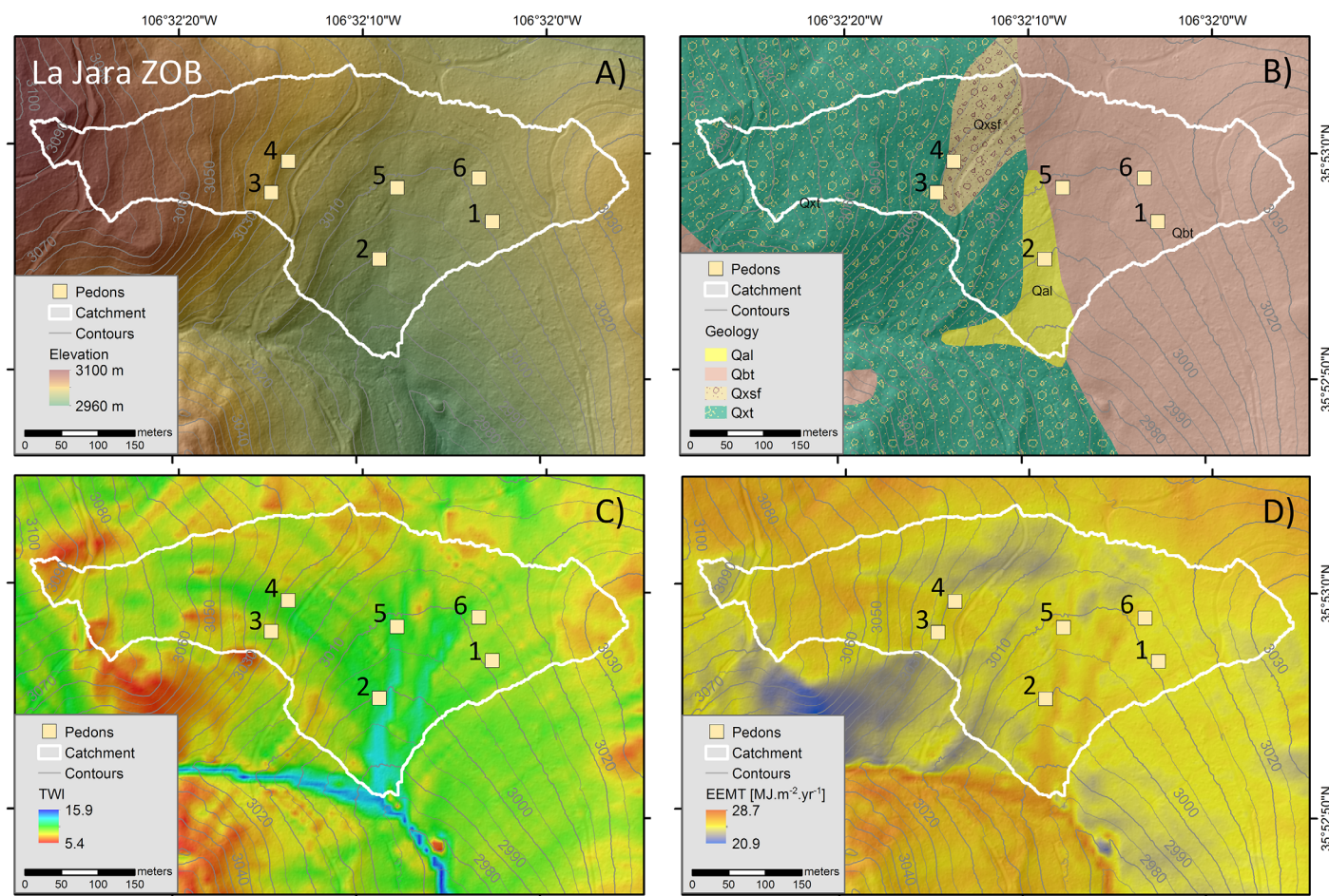


Figure 3. Landscape characteristics of the La Jara Zero Order Basin (ZOB; location within the larger La Jara catchment shown in Figures 1 and 2). (a) Topography; (b) Geology [Goff *et al.*, 2005, 2006a, 2006b; Goff, 2009]. See Figure 2 for explanation of abbreviations for geologic units; (c) Topographic wetness index (TWI), and (d) effective energy and mass transfer (EEMT_{TOPO}) [Rasmussen *et al.*, 2015]. Numbered locations represent the six instrumented pedons installed in 2011 with soil solution (Prenart and passive capillary or “wick”) samplers.

materials during resurgence of the dome. In addition, there is Quaternary alluvium in the center of the ZOB near the outlet.

ZOB soils consist of Alfisols, Mollisols, and Inceptisols [Broxton *et al.*, 2009], and predominantly contain quartz, alkali feldspars, biotite, and muscovite (from dust), Ca-clinoptilolite, montmorillonite (diagenetic or neogenic), and kaolinite [Vázquez-Ortega *et al.*, 2016]. There is also a chemical signature of modern dust (i.e., Eu-anomaly) in the upper 5–10 cm of most soil profiles in the ZOB [Vázquez-Ortega *et al.*, 2016], as well as volcanic ash based on ²³⁰Th enrichment in shallow soils [Huckle *et al.*, 2016]. Soil total organic carbon (TOC) content is highest in the O-horizon, except for Pedon 5, located in the center swale of the ZOB (Figure 3a) where TOC content was highest at middepths (25–59 cm) [Vázquez-Ortega *et al.*, 2016].

2.1.2. Hydrology

The hydrologic response of La Jara Creek is typical of snowmelt-dominated catchments. Stream discharge typically peaks in late March to early April corresponding to spring snowmelt, and a gradual recession lasts until the onset of the following spring snowmelt. Summer monsoon precipitation events in July through September occasionally lead to small, sporadic increases in stream discharge, but these are minimal compared to the snowmelt pulse, as much of the summer precipitation returns to the atmosphere via evapotranspiration [Broxton *et al.*, 2009; Liu *et al.*, 2008b; Zapata-Rios *et al.*, 2015a]. Winter base flow is low, rarely exceeding 0.23 mm d⁻¹ (area normalized). Total annual discharge strongly correlates to the maximum snow water equivalence (max SWE) and duration of snow on the ground [Zapata-Rios *et al.*, 2015a].

Large interannual variations in max SWE, duration of snow cover, precipitation, and stream discharge were observed over the study period in La Jara catchment. Water Year (WY; defined as 1 October to 31

Table 1. Weathering Fluxes Calculated From Solid (Soil) and Aqueous (Soil Water and Stream Water) Phase Geochemistry

	Soil Age (Years)	Curvature	Dominant Lithology	^a Water Flux (L m ⁻²)	TWI ^b	^b EEMT _{TOPO} (MJ m ⁻² yr ⁻¹)	**Na Weathering Rate (mmol m ⁻² yr ⁻¹)	<i>stdev</i> (mmol m ⁻² yr ⁻¹)	Si Weathering Rate (mmol m ⁻² yr ⁻¹)	<i>stdev</i> (mmol m ⁻² yr ⁻¹)
ZOB soils										
<i>Pedon 1</i>	16,900	Planar	Tuff	54	9.61	25.07	2.6	1.0	68	27
<i>Pedon 2</i>	21,200	Concave	Alluvium	101	10.84	24.97	6.2	2.5	282	113
<i>Pedon 3</i>	21,000	Convex	Rhyodacite	48	8.38	24.67	1.3	0.5	609	245
<i>Pedon 4</i>	25,400	Concave	Sandstone	39	10.35	25.15	7.4	3.0	528	212
<i>Pedon 5</i>	21,000	Concave	Tuff	108	10.42	24.91	0.0	0.0	20	8
<i>Pedon 6</i>	16,800	Concave	Tuff	85	9.23	25.11	7.2	2.9	54	22
Avg. All Pedons							4.1	1.7	260	105
							Na Solute Fluxes (mmol m ⁻² yr ⁻¹)	<i>stdev</i> (mmol m ⁻² yr ⁻¹)	Si Solute Fluxes (mmol m ⁻² yr ⁻¹)	<i>stdev</i> (mmol m ⁻² yr ⁻¹)
ZOB Soil Water										
Avg. 2011–2012							14	7.5	31	6.7
La Jara Stream Water										
^b WY 2010							15	0.5	38	0.01
WY 2011							5.5	0.1	12	0.1
WY 2012							8.9	0.1	27	0.2
Avg. All WYs							9.7	0.2	26	0.1

^aCumulative maximum water fluxes through pedons in WY 2012 measured using wick lysimeters [Vázquez-Ortega et al., 2016].

^bTWI = topographic wetness index; EEMT_{TOPO} = Effective Energy and Mass Transfer [Rasmussen et al., 2015]; WY = Water Year.

**Average values for Na and Si weathering rates and solute fluxes are reported with standard deviation (*stdev*) error associated with parameter variability.

September) 2010 was a relatively “wet year” with 642 mm of annual precipitation (63% as winter precipitation) and a deep snowpack (302 mm of max SWE) that lasted from 7 December to 28 April. WY 2011 was “dry” with 591 mm of annual precipitation (only 40% as snow), and an ephemeral snowpack in many parts of the watershed with only 48 mm of max SWE that persisted from 16 December to 28 March. WY 2012 and 2013 were “wetter” than WY 2011 with 705 and 668 mm of annual precipitation, respectively, but had a thinner snowpack (only 110 and 85 mm of max SWE, respectively) that melted earlier (snowpack only persisted until 8–11 April, respectively) than in WY 2010 [Perdrial et al., 2012; Zapata-Rios et al., 2015a]. A snow-on LiDAR flight made on 1 April 2010 [Harpold et al., 2014] showed that snow depths on the southeast-facing ZOB hillslope were 12% larger (average of 53 cm) compared to the southwest-facing hillslope (average of 47 cm), illustrating variability in the snowpack as a function of aspect. In the subhumid study area, over 92% of the precipitation that infiltrates is utilized by plants and returned to the atmosphere via transpiration [Zapata-Rios et al., 2015a]. Discharge on average accounts for only 8% of total annual precipitation, with base flow being the largest component of discharge (over 90% of total discharge) [Zapata-Rios et al., 2015a].

Previous studies suggest that the majority (71–86%) of streamflow in La Jara Creek comes from precipitation that infiltrates (vertically) into the subsurface and moves laterally to the stream along horizontal flow paths near the soil-bedrock interface [Liu et al., 2008a]. The stable isotope signatures ($\delta^{18}\text{O}$ and δD) of water indicate snowmelt is the dominant source of water to groundwater reservoirs contributing to stream flow year round [Liu et al., 2008a, 2008b; Zapata-Rios et al., 2015b]. This result is consistent with other studies showing the predominance of winter precipitation on groundwater recharge and stream base flow in western montane catchments [Bales et al., 2006; Henderson and Shuman, 2010]. There is little chemical and isotopic evidence of direct overland flow during snowmelt or summer monsoons contributing to La Jara Creek [Liu et al., 2008a; Perdrial et al., 2014a]; the well-drained soils around Redondo Peak likely enhance infiltration and decrease surface run-off [Liu et al., 2008a]. Infiltration of spring snowmelt connects the hillslopes to the stream, flushes shallow soils, and delivers soil-derived dissolved organic carbon (DOC) and rare earth elements and yttrium (REY), possibly from reductive dissolution of Fe and Mn oxide minerals, to La Jara Creek [Perdrial et al., 2012; Vázquez-Ortega et al., 2015]. During the drier, summer and fall periods, La Jara Creek contains more microbially derived DOC, likely from reworking of plant-derived organic carbon in groundwater and/or the stream [Perdrial et al., 2014a].

At the pedon-scale in the ZOB in La Jara catchment, Vázquez-Ortega et al. [2016] show seasonal differences in water fluxes through soil profiles based on landscape position (determined using 1 and 10 m LiDAR data sets, as described in Vázquez-Ortega et al. [2016]; Table 1) that influences transport of DOC. Soils in concave

positions had the highest cumulative annual water and DOC fluxes over the entire soil profile, and high water and DOC fluxes in both shallow (3 cm) and deep (54 cm) soil horizons, with lower fluxes at middepths (17 cm), suggesting lateral subsurface water transport in shallow and deeper soil horizons in seasonally saturated soils [Vázquez-Ortega *et al.*, 2016]. In contrast, soil profiles in planar hillslope positions exhibited the highest cumulative annual water and DOC fluxes in the shallowest soil horizons, which decrease with depth, suggesting dominantly vertical water transport [Vázquez-Ortega *et al.*, 2016]. A recent geophysical survey in the ZOB shows that the mobile soil layer is uniformly thick (1 ± 1 m) across the catchment, and the depth to unweathered bedrock is slightly higher on the southwest-facing slope (49 ± 10 m) compared to the southeast-facing slope (42 ± 6 m) [Olyphant *et al.*, 2016]. The thinnest regolith is found above the valley bottom [27 ± 4 m].

A distribution of transit times have been observed in surface water in La Jara catchment dependent on the age tracer used and reflective of contributions of water from variable flow paths, as shown in other studies [e.g., McGuire and McDonnell, 2006; Heidbüchel *et al.*, 2013]. Transit times of La Jara Creek base flow range from 110 to 163 days based on stable water isotopes [Broxton *et al.*, 2009], and spring waters range from 1.5 to 12.3 years based on tritium analyses [Zapata-Rios *et al.*, 2015b]. Seasonal changes in $^{234}\text{U}/^{238}\text{U}$ activity ratios suggest displacement of older waters stored in the catchment to La Jara Creek during spring snowmelt, compared to drier periods [Huckle *et al.*, 2016].

Two stand-replacing wildfires affected the VCNP during the study period: the Las Conchas fire (burned from 26 June to 3 August 2011) and the Thompson Ridge fire (started on 31 May 2013). Although the Las Conchas fire did not extend into the La Jara catchment, ash fall may have influenced the catchment chemistry. The Thompson Ridge fire affected much of the La Jara catchment with mid to high severity burned areas. This study includes data up to the day (30 May 2013) prior to the start of the Thompson Ridge fire to investigate “prefire” conditions only; future studies will investigate the impacts of the fire on catchment hydrobiogeochemistry.

The Valles Caldera is still hydrothermally active, with hot springs and fumaroles on the western and northern parts of the VCNP [e.g., Vuataz and Goff, 1986]; however, there is no evidence of geothermal waters (e.g., elevated solute concentrations) or gases (e.g., elevated $[\text{CO}_2]$), influencing the chemistry of La Jara catchment [Liu *et al.*, 2008a].

2.2. Sample Collection and Analysis

2.2.1. Bedrock

Outcrop samples of bedrock that represent the two dominant lithologies (Bandelier Tuff and rhyodacite) were collected near the ZOB in summer 2010. Rock samples were crushed and the least weathered sections selected for geochemical analyses. Elemental composition of bedrock samples was determined following lithium metaborate/tetraborate fusion by dissolution of the pellet in nitric acid and analysis of the solution by inductively coupled plasma (ICP) optical emission spectrometry (-OES) and mass spectrometry (-MS) (Activation Laboratories, Ancaster, Ontario).

2.2.2. Soils

Six pedons were excavated in the ZOB in September 2010 and instrumented with soil solution (Prenart and passive capillary or “wick”) samplers, creating two east-west trending transects (Figure 3a) as part of the JRB-CZO [Perdrial *et al.*, 2012, 2014b]. Soil samples were collected in all of the pits from each genetic horizon, sealed in Ziploc™ bags, and stored at 4°C. The soils were air dried, sieved to recover the <2 mm fraction, mixed for homogeneity, and stored at room temperature. Five grams of each sample were mixed with a flux consisting of lithium tetraborate and lithium metaborate, and fused. Total elemental concentrations were analyzed using ICP-OES and ICP-MS (Si, Ca, Na, Mg, K, Fe, Al, Mn, and Ti).

For determination of Ge concentrations, soil samples were ashed for 30 min at 500°C in porcelain crucibles to oxidize organic matter. Fifty milligrams of the ashed material was measured into a disposable graphite crucible and mixed with 300 mg of flux consisting of a 1:1 ratio of lithium tetraborate and lithium metaborate. These mixtures were fused in a muffle furnace at 1000°C for 10 min. The samples were removed from the oven, swirled, and then placed in the oven for another 10 min to sinter the samples. The bead produced was put in 60 mL acid-washed HDPE bottles that were 2/3 filled with 1 M HNO_3 and placed in a shaker until completely dissolved (~15 min). Samples were then hand-filtered with a 0.45 μm filter into another 60 mL acid-washed HDPE bottle to remove any residual carbon particles and diluted with Milli-Q water to a

Ge concentration of $\sim 250 \text{ ng L}^{-1}$. Both digested soil samples and water samples were spiked with an enriched ^{70}Ge tracer solution and allowed to equilibrate for at least 24 h. Spiked samples were analyzed by isotope dilution hydride generation ICP-MS in the Department of Earth and Atmospheric Sciences, Cornell University, Ithaca [Blecker *et al.*, 2007]. Typical uncertainties for [Ge] are $\leq 2\%$. For calculation of Ge/Si ratios, silica concentrations in selected water samples were determined using the “molybdate blue” spectrophotometry method [Mortlock and Froelich, 1996]. The soil geochemistry data for the sampled pedons are available through EarthChem [Rasmussen and Chorover, 2017].

Chemical depletion or enrichment (τ) values for soils relative to the parent, bedrock materials were determined using titanium (Ti) as the immobile element, following Brimhall and Dietrich [1987] and Chadwick *et al.* [1990] (equation (1)):

$$\tau_{j,w} = \left(\frac{C_{j,w}}{C_{j,p}} \times \frac{C_{i,p}}{C_{i,w}} \right) - 1 \quad (1)$$

in which C is the mass concentration (mg kg^{-1}), j is the element in question, i is the immobile element (Ti), w is the weathered material, and p is the parent material. To account for differences in the underlying geology between the six pedons and geologic complexity across the ZOB, we used the bottom most soil horizon sampled in each pedon as an estimate of the local parent materials. Using the lower most horizon as reference provides a conservative (minimal) estimate of chemical depletion and focuses only on shallow CZ weathering, particularly if deeper weathering fronts exist. Tau (τ) > 0 indicates gain of an element with respect to the immobile element in the parent material, whereas $\tau < 0$ indicates loss of an element with respect to the immobile element in the parent material.

Na and Si weathering rates were determined from chemical depletion-enrichment profiles by first calculating the strain (ε) to determine the volumetric change [Brimhall and Dietrich, 1987]:

$$\varepsilon_{i,w} = \left(\frac{\rho_p C_{i,p}}{\rho_w C_{i,w}} \right) - 1 \quad (2)$$

where ρ_p is the bulk density of the parent bedrock and ρ_w is the bulk density of the soil. Bandelier Tuff bulk density values vary with degree of welding, with locally measured values for moderately welded tuff comparable to that observed in the ZOB ranging from 1.6 to 1.9 g cm^{-3} [Purtymin, 1967]. Well-sorted sandstone bulk density is on the order of 2.6 g cm^{-3} , while the alluvial parent material is closer to 1.6 g cm^{-3} [Grossman and Reinsch, 2002]. Given the variability in the parent materials in the ZOB and dominance of volcanic bedrock, we used an average bulk density value of 1.8 g cm^{-3} in equation (2), and used the full range of values (1.6 – 2.6 g cm^{-3}) in our error estimation calculations.

To determine the total mass flux of Na and Si ($C_{j,w}$), the elemental mass flux ($m_{j,\text{flux}}$, g cm^{-2}) was calculated for each soil horizon [Brimhall and Dietrich, 1987; Egli and Fitze, 2000; Heckman and Rasmussen, 2011]:

$$m_{j,\text{flux}} = \rho_p C_{j,p} \tau_w [z_w (1 - \eta_w)] * \left(\frac{1}{\varepsilon_{i,w} + 1} \right) \quad (3)$$

where z_w is horizon thickness (cm), and n_w is the volumetric percent rock fragment content ($\text{cm}^3 \text{ cm}^{-3}$). The $m_{j,\text{flux}}$ values for the individual soil horizons were summed for each pedon to determine the total Na or Si flux from the pedon that has occurred during pedogenesis ($m_{j,\text{flux}}$ total, g cm^{-2}). The total Na and Si max flux from each pedon was converted to moles cm^{-2} and divided by the soil mean residence time to determine weathering rates (moles $\text{cm}^{-2} \text{ yr}^{-1}$). The flux calculations do not account for mineral surface area. Any dust or precipitation contributions to the Na and Si weathering rates were also not accounted for in equation (3), as dust and precipitation inputs of Na and Si were considered negligible (as described in section 3.1).

The soil residence time for each pedon was estimated by dividing the thickness of the soil by the watershed-averaged erosion rate derived from the inventory of cosmogenic ^{10}Be in stream sediments for La Jara reported by Orem and Pelletier [2016] ($59.4 \pm 3.6 \text{ m Myr}^{-1}$). The error associated with soil residence time was included in the error estimation of the Na and Si weathering rates above. Estimates of soil residence time rely on an assumption that soil thickness does not change through time, i.e., that the rate of lowering of the soil-saprolite boundary occurs at the same rate that the landscape is lowered by erosion.

The negative feedback between soil production rates and soil thickness (in which an increase in erosion rates tends to thin soils, thereby triggering enhanced soil production rates or, conversely, a thickening of soils and a decrease in soil production rates in response to a decrease in erosion rates) is one reason why the soil thickness steady state assumption is likely to hold, at least approximately, in many landscapes [e.g., *Heimsath et al.*, 2001]. Previous work has suggested that erosion rates may have increased at the Pleistocene-Holocene transition and into the Holocene [*Reneau et al.*, 1996]. Relatively low erosion rates in the latest Pleistocene relative to the Holocene could have had the effect of making the soils slightly younger than estimated here, because some of the ^{10}Be accumulation associated the Holocene may have occurred under slower erosion rates during the latest Pleistocene.

2.2.3. Dust

Dust samples were collected from two dust traps installed at high (3242 m) and low (2825 m) elevations on Redondo Peak (Figure 1). Traps were installed on top of a 1.5 m above-ground metal post and consisted of a circular cake pan (area of 450 cm²), filled with glass beads, and covered in wire mesh [*Reheis et al.*, 1999]. Bulk dust samples were collected from 26 July to 15 October 2011, by rinsing the pan and marbles with deionized water into a HDPE bottle. Samples were centrifuged and air-dried before being subjected to a HF-HCl-HNO₃ digestion and analyzed by ICP-MS. Acid digestion (with HF, HCl, and HNO₃) used for dust samples and lithium metaborate fusion used for soil samples should report the same Si concentrations when the analyses are both done correctly [*Jones and Dreher*, 1996; *Arslan et al.*, 2000; *LeBond et al.*, 2011].

2.2.4. Precipitation, Soil Water, and Surface Water

Snow was collected from snow-pits weekly from 13 March to 3 May 2011, stored in new 1 gallon Ziploc™ bags, kept frozen in the field, and allowed to melt overnight in the laboratory at the University of Arizona (UA) prior to filtering. Bulk rainwater samples were collected in DI-washed HDPE bottles at two sites (one located within the ZOB and one near the La Jara catchment outlet flume; Figure 1) over the period of 1 week during the summer monsoon season. Soil water samples were collected in acid-washed HDPE bottles from Prenart lysimeters installed at multiple depths in each of the six pedons in the ZOB from mid-March to the end of May 2011 (Figure 3a). Larger volumes of water were collected from the passive capillary samplers versus Prenart suction lysimeters, installed in the same locations, however previous studies have shown that wick samplers introduce contamination for Si and major base cations [*Perdrial et al.*, 2012, 2014b]. Surface water samples were collected monthly from the La Jara Creek flume during the presnowmelt and summer dry periods, and weekly (except in 2010) during the spring snowmelt and summer monsoon seasons from January 2010 to May 2013. No surface water samples were collected during the winter due to inaccessibility issues, but flows are normally low during this period because of frozen snowpack accumulation. Surface water samples were also collected from a flume at the outlet of the ZOB, which drains into the upper portion of La Jara Creek, from 13 March to 4 May 2011. Only a few stage measurements were available for the ZOB during this period due to freezing conditions, thus discharge was estimated using a correlation between volumetric moisture content (at the pedon scale) and discharge, as reported in *Vázquez-Ortega et al.* [2015].

Temperature, pH, dissolved oxygen, and conductivity of surface waters were measured in the field using an Accumet AP84 (Fisher Scientific) multiprobe. Surface water samples for cation chemistry and trace metals were collected in acid-washed HDPE bottles. Samples for dissolved inorganic carbon (DIC), DOC, and anion chemistry were collected in combusted amber glass bottles. Bottles were rinsed three times with stream water, filled to eliminate headspace, and stored cool (4°C) until samples were processed in the laboratory.

All water samples were packed on ice and sent overnight to UA to be filtered within 2 days of collection using 0.45 μm nylon filters. Sample aliquots for DIC and DOC were filtered through combusted 0.7 μm glass-fiber filters. Sample aliquots for major and minor cations, and Ge were preserved in acid-washed HDPE bottles with concentrated Optima grade nitric acid. All water samples were stored at 4°C prior to analysis. Major and minor cations (Si, Ca, Na, Mg, K, Fe, Al, and Mn) were analyzed by ICP-MS in the Arizona Lab for Emerging Contaminants (ALEC) at the UA. Dissolved inorganic carbon and DOC were analyzed on a Shimadzu TOC-VCSH Carbon analyzer (Shimadzu Scientific Instruments, Columbia, MD) in ALEC. The full data set of soil solution chemistry is available through EarthChem [*Chorover et al.*, 2017]. Spring water and La Jara Creek chemistry data are available through HydroShare [*McIntosh et al.*, 2017].

To determine Ge concentrations of water samples, a quantity of enriched ^{70}Ge tracer solution sufficient to increase the $^{70}\text{Ge}/^{74}\text{Ge}$ ratio to $\approx 5\text{--}10$ (estimated from the Si concentration) was added 6–8 mL of sample.

The sample was then evaporated to about half the original volume (3–4 mL). Samples were weighed before and after to determine the exact amount of water evaporated. Samples were then prepared and analyzed using the same method as described for the soil digests. Due to insufficient sample volume, Ge concentrations could not be determined for the soil waters.

Stream water solute fluxes were determined by estimating a daily Na and Si flux for days with stream composition observations and by calculating a flow-weighted mean solute concentration for each year using the mean flow method [Godsey *et al.*, 2009]. Flux estimation errors were calculated on the basis of maximum analytical error of 5% and a discharge measurement error of 10%. Sampling bias of flux estimations was included with Tukey's jackknife variance estimation [Efron and Stein, 1981]. To calculate solute fluxes from soil pore waters, maximum cumulative water fluxes from wick lysimeters (observed in WY 2012, and reported in Vázquez-Ortega *et al.* [2016]) were paired to Na and Si concentrations from suction lysimeter samples. Wick lysimeters exert a negative pressure of 5 kPa (from height of the hanging water column) during solution collection, and they exhibit high hydraulic conductivity, capturing the maximum water flux through soil profiles, whereas Prenart suction lysimeters are collected at 40 kPa and so may draw in more tightly-held, and older water that may be chemically enriched, hence, the solute flux calculations can be considered maximum estimates.

2.2.5. Landscape Characteristics

The ZOB is south-facing with dominant SW and SE facing slopes separated by a concave swale that has surface flows only observed near the ZOB outlet flume during spring snowmelt. Vázquez-Ortega *et al.* [(2016) previously defined the land surface curvature and topographic wetness indices (TWI) for the six pedons in the ZOB based on a 1 m LiDAR data set [Guo *et al.*, 2010]. Pedon 1 is in a planar position, Pedon 3 is in a convex position, and Pedons 2, 4, 5, and 6 are in concave landscape positions (Table 1). Effective Energy and Mass Transfer (EEMT) was determined using the method described in Rasmussen *et al.* [2015] that accounts for local topographic controls on subsurface water redistribution, evapotranspiration, and primary productivity, referred to as EEMT_{TOPO}. EEMT provides a metric of the chemical energy and heat transfer to the subsurface, in the form of reduced carbon associated with primary productivity and effective precipitation, respectively, that has the potential to perform work in the CZ. Previous studies have shown a positive relationship between EEMT and mineral weathering fluxes for springs draining different aspects of Redondo Peak [Zapata-Rios *et al.*, 2015b]. The TWI and EEMT_{TOPO} were computed using the 1 m LiDAR data set [Guo *et al.*, 2010] upscaled to 10 m to smooth the uneven surface generated from the LiDAR scan while preserving principal topographic features in the study area.

3. Results

3.1. Bedrock, Soils, and Dust

Pedons 1 and 6, on the southwest-facing side of the ZOB, are underlain by the Bandelier Tuff (Figure 3b). They are in planar and concave landscape positions, respectively, and have relatively low topographic wetness index (TWI) values and intermediate maximum cumulative water fluxes (Table 1 and Figure 3c) with likely dominant vertical water transport based on solid-phase REY and water flux patterns with depth [Vázquez-Ortega *et al.*, 2016]. Pedon 4 is underlain by sandstone and is in a concave landscape position on the southeast-facing slope with a relatively high TWI, but the lowest cumulative water flux (Table 1). Pedon 5 is underlain by Bandelier Tuff and Pedon 2 is underlain by alluvium. Both pedons 5 and 2 are in the convergent zone (concave position) of the ZOB, in a meadow area, and have the highest TWI, maximum cumulative water flux (Table 1), and DOC fluxes, which are primarily lateral during periods of seasonal saturation [Vázquez-Ortega *et al.*, 2016]. Pedon 3, on the southeast-facing side of the ZOB, is underlain by the Tschicomoma Formation rhyodacite and contains evidence of colluvial transport. Pedon 3 is in a convex position, has the lowest TWI value, and a relatively low maximum cumulative water flux that is invariant with depth (Table 1) [Vázquez-Ortega *et al.*, 2016]. There is little variation in EEMT_{TOPO} values between the six pedons in the ZOB (Figure 3d) and no significant difference with landscape position and aspect (Table 1). Estimates of soil age or residence time for the six pedons range from 16.5 to 25 kyr, with higher values on southeast-facing slopes and the valley center compared to southwest-facing slopes.

Despite differences in the underlying bedrock geology, landscape positions, TWI, and water fluxes, there are no major differences in chemical depletion or enrichment (τ) values, except for Si, Fe, and Al, between the six soil profiles below 10 cm (Figures 4–6). All of the pedons show an enrichment in Ca, Mg, and Sr in

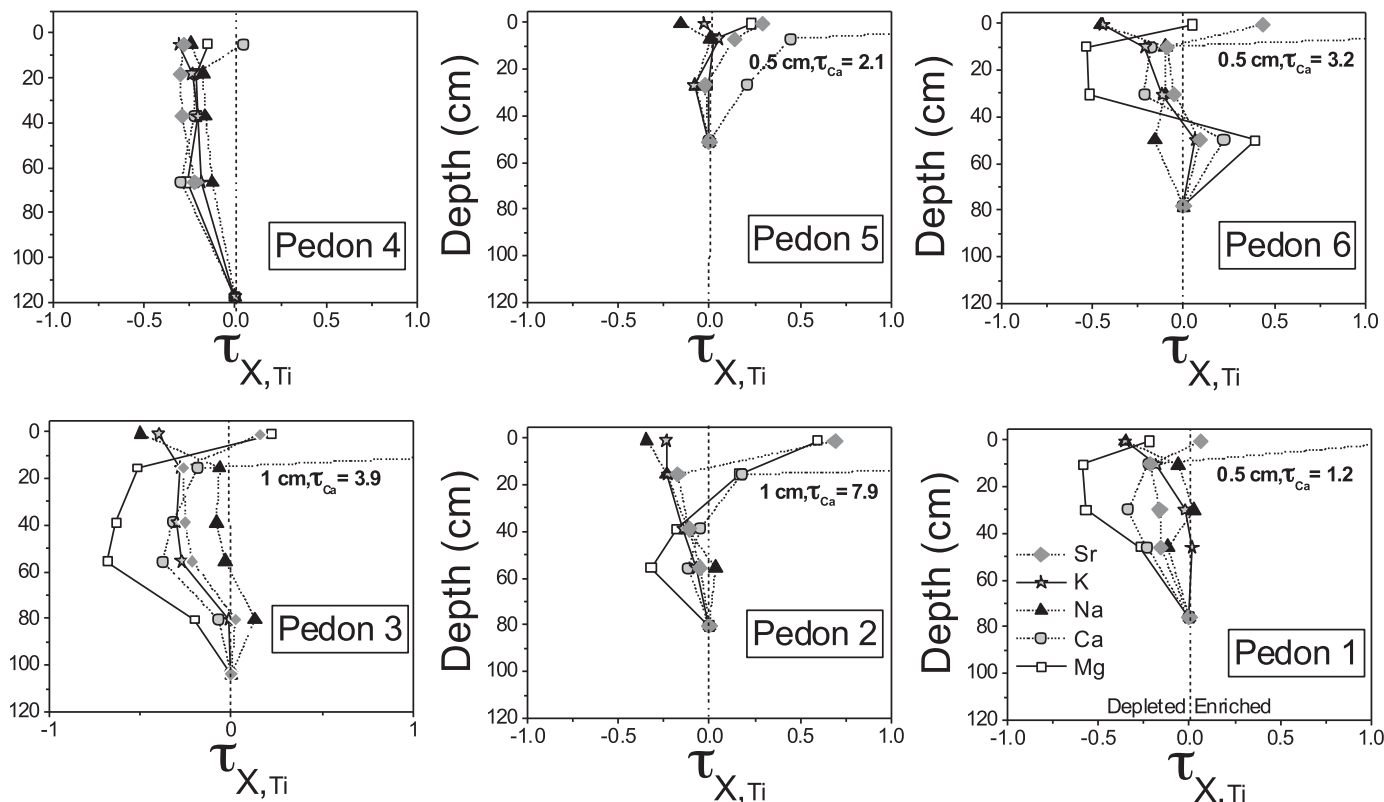


Figure 4. Elemental depletion profiles of major cations from the six pedons in the Mixed Conifer Zero Order Basin (MCZOB) in La Jara catchment. Positive tau (τ) values indicate the element is enriched compared to the bedrock, while negative τ values indicate depletion.

the top most horizon (<10 cm); the enrichment in Ca is observed to at least ~ 30 cm depth in Pedon 5 (Figure 4). There is also a pronounced enrichment in Mn in the top most horizon of all pedons, except Pedon 4, which shows the highest Mn enrichment at ~ 20 cm depth (Figure 5). Beneath ~ 10 cm, Mn, Mg, Ca, and Sr are depleted relative to the deepest soil horizon. Iron and Al are also depleted compared to the deepest soil horizon, except for a slight enrichment in the O-horizon associated with the enrichment in Mn (Figure 5). There also appears to be slightly more depletion of Fe and Al below 10 cm in pedons located on the hill-slopes, compared to pedons beneath the concave center of the ZOB. Na, K, and Si are the most depleted in the shallow horizons with increasingly less depletion with depth (Figure 4). Si appears to be depleted to greater depths in Pedons 2, 3, and 4, which are underlain by alluvium, rhyodacite, and sandstone, respectively, compared to Pedons 1 and 6, which are underlain by welded tuff (Table 1; Figure 6). Pedons 2, 3, and 4 are also located near the ZOB outlet in the central swale and on the NE-facing slope, whereas pedons 1 and 6 are located on the SW-facing slope. Pedon 5 shows little depletion of Si (and other constituents), likely because of using a relatively shallow soil horizon as the parent material in equation (2) (Figure 6). Ge shows a similar pattern with depth as Si, with a slight enrichment in the top two horizons in Pedons 2 and 3 (Figure 6).

Na and Si were chosen to calculate weathering rates for soils (equation (3)) as they are dominant elements in the volcanic bedrock in the area and are thought to be transported relatively conservatively to stream-flow [Zapata-Rios *et al.*, 2015b]. In addition, Na and Si are considered good proxies for plagioclase and silicate weathering, respectively [e.g., White *et al.*, 1998]. Na and Si weathering calculations did not include dust contributions, as dust in the study area contained relatively little Na and Si (20 and 119 mmol kg⁻¹, respectively) compared to the tuff and rhyodacite (165 and 1432 mmol kg⁻¹ Na, and 10,747 and 11,800 mmol kg⁻¹ Si, respectively). In addition, although the mineral material of the O-horizon does appear to be largely composed of dust, based on its mineralogy and geochemistry, the dust in the O-horizon represents only a small fraction of the pedon mass because it is a relatively thin zone (top 5 cm) of material on the surface of the pedon, and has a low bulk density relative to the rest of the pedon. Furthermore, we assumed

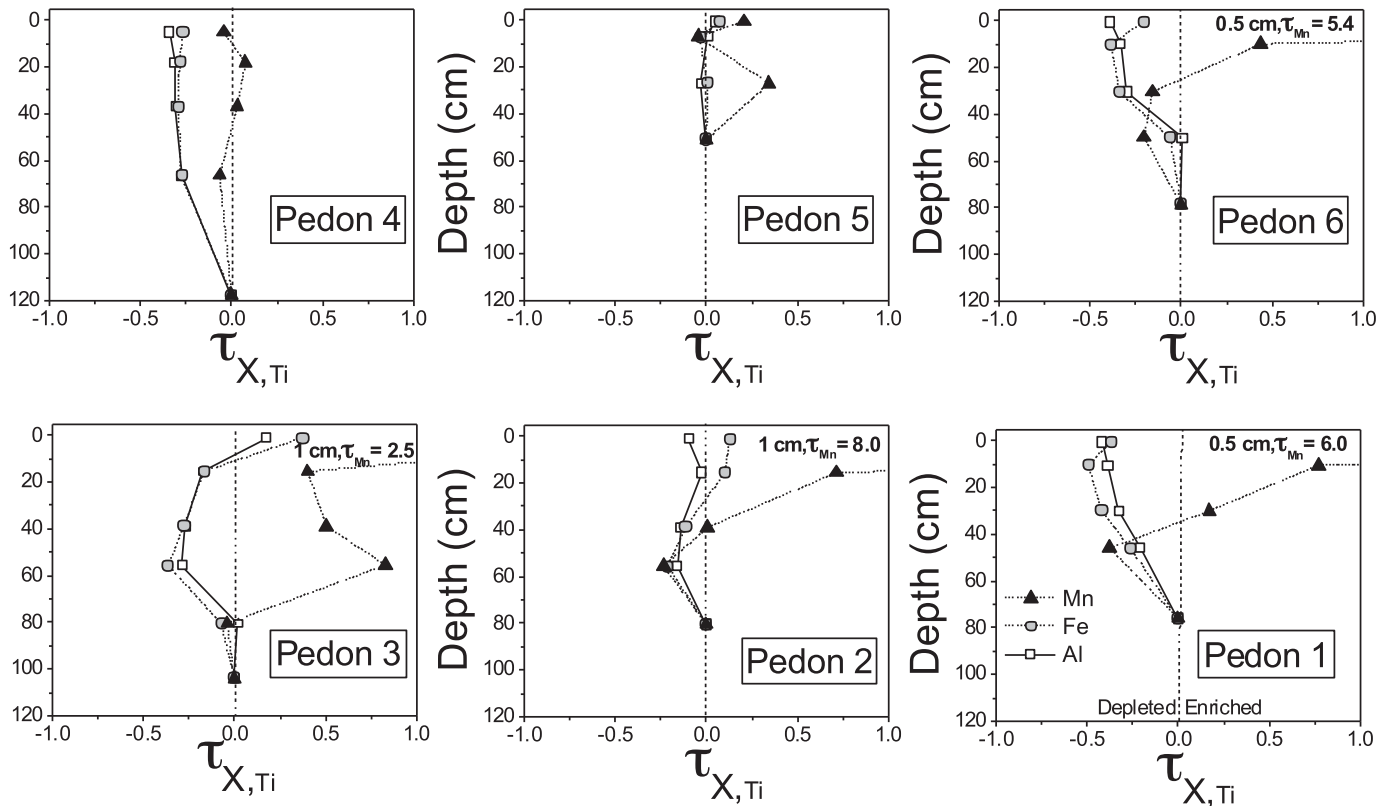


Figure 5. Elemental enrichment/depletion profiles of total Mn, Fe, and Al from the six pedons in the Mixed Conifer Zero Order Basin (MCZOB) in La Jara catchment.

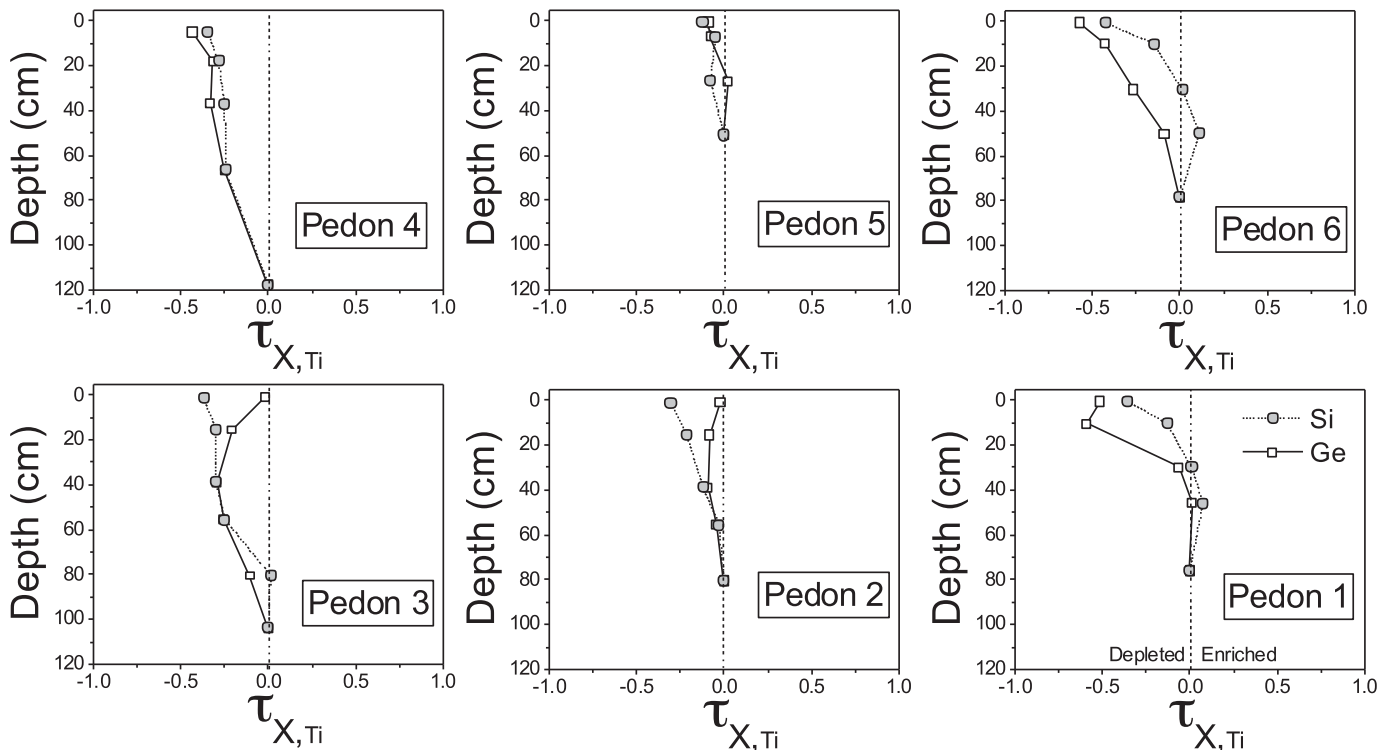


Figure 6. Elemental enrichment/depletion profiles of Si and Ge from the six pedons in the Mixed Conifer Zero Order Basin (MCZOB) in La Jara catchment.

Table 2. Summary of pH and Solute Chemistry for Various Water Types Sampled in La Jara Catchment

Water Type	^a n	pH	^b DIC	DOC	Si	Na	K	Ca	Mg	Sr
Precipitation	111	5.5 (0.9)	126 (126)	314 (429)	11 (20)	6.4 (8.3)	12 (9.7)	24 (28)	7.3 (17)	0.14 (0.28)
Soil water	37	6.8 (0.6)	514 (752)	1764 (1246)	229 (118)	132 (164)	60 (141)	294 (372)	88 (212)	0.55 (0.61)
ZOB surface water ^c	62	6.8 (0.3)	215 (63)	923 (228)	317 (72)	78 (20)	71 (42)	184 (43)	27 (5)	0.37 (0.07)
Shallow groundwater	38	7.3 (0.3)	547 (64)	223 (108)	312 (113)	143 (60)	31 (28)	135 (59)	27 (10)	0.3 (0.12)
Deep groundwater	68	6.6 (0.4)	379 (68)	81 (34)	483 (227)	240 (46)	43 (38)	135 (46)	25 (15)	0.29 (0.10)
Stream (snowmelt)	31	6.9 (0.3)	267 (33)	235 (99)	337 (75)	114 (18)	23 (8.5)	121 (35)	21 (5.6)	0.26 (0.03)
Stream (base flow)	12	6.8 (0.3)	346 (140)	138 (66)	292 (80)	101 (17)	17 (6.9)	94 (34)	20 (1.5)	0.23 (0.02)

Water type	n	Fe	Al	Mn	Ge	Cl	SO ₄
Precipitation	111	0.28 (0.60)	0.76 (1.4)	0.69 (1.4)	NA	21 (79)	8.9 (11)
Soil water	37	4.2 (15)	3.1 (4.2)	0.18 (0.27)	NA	101 (90)	44 (18)
ZOB surface water ^c	62	2.8 (0.7)	7.5 (2.6)	0.16 (0.37)	NA	40 (24)	92 (20)
Shallow groundwater	38	0.73 (1.2)	2.5 (4.6)	0.3 (1.8)	287 (206)	41 (23)	42 (18)
Deep groundwater	68	2.7 (9.1)	2.2 (2.2)	0.02 (0.05)	NA	19 (5.0)	27 (3.1)
Stream (snowmelt)	31	1.0 (1.2)	3.3 (2.6)	0.02 (0.01)	296 (446)	26 (17)	33 (6.8)
Stream (base flow)	12	1.2 (1.5)	1.8 (1.3)	0.01 (0.01)	49 (55)	20 (7.5)	30 (2.9)

^an = number of samples; NA = not analyzed.

^bMean values (in micromoles L⁻¹ except for Ge, which is in picomoles L⁻¹) are shown with one standard deviation in parentheses.

^cData only available for spring snowmelt 2011.

any error associated with not including dust in the weathering flux calculations, and thus overestimating weathering rates, would be within the error of the calculations due to other factors, such as variability in parent materials. This assumption was confirmed when we compared Na and Si weathering fluxes with and without including the O-horizon and found no significant difference. Dust samples contained no detectable Ge. Calcium, Mg, and trace element concentrations, except for Mn, were lower in dust compared to soil and bedrock samples.

Chemical weathering rates for Na and Si ranged from 0 to 7.4 (±3) and 20 (±8) to 609 (±245) mmol m⁻² yr⁻¹ for the six pedons, respectively (Table 1). Higher Si weathering rates were seen for pedons underlain by rhyodacite (Pedon 3), sandstone (Pedon 4), and alluvium (Pedon 2), compared to tuff (Pedons 1, 5, and 6); the higher Si weathering fluxes for Pedons 2, 3, and 4 may also be a function of landscape position, as these pedons are located in the concave center of the ZOB and on the NE-facing hillslope, respectively. We did not attempt to area-normalize the Si weathering rates for each lithology given the complexity of underlying parent materials. There was no significant difference between Na weathering rates for pedons underlain by different parent materials (Table 1). We also found no relationship between Na or Si weathering rates and TWI, EEMT_{TOPO}, or cumulative water fluxes (Table 1).

3.2. Precipitation

All water types investigated, including precipitation, are dominated by Si, Ca, Na, Mg, and HCO₃ (Table 2). Rain and snow are slightly acidic (pH 5.5 average) and dilute, with lower solute concentrations, except for Mn, compared to soil waters, groundwater, and surface waters. Mn likely originates from atmospheric deposition (dust) related to anthropogenic inputs [Herndon et al., 2011]. Ge concentrations in rain and snow samples were below detection, as is commonly observed [Kurtz et al., 2002, 2011; Derry et al., 2006; Lugolobi et al., 2010].

3.3. Soil Solution

Soil waters have the highest solute concentrations of all the water types sampled in La Jara catchment, and have the highest DOC concentrations (Table 2). The pH values for soil waters (6.8 average) are similar to all other water types, except precipitation. Prenart lysimeters installed in Pedons 2, 5, and 6 produced the largest volume of soil waters sampled for chemical and isotopic analyses, consistent with Pedons 2 and 5 being situated in the concave center of the ZOB with higher subsurface (lateral) cumulative water flux (Table 1) [Vázquez-Ortega et al., 2015]. Only limited soil waters were produced from the other three lysimeters. Thus, we focus our study on Pedons 2, 5, and 6.

Concentrations of Ca and Mg in soil pore waters are highest near the surface (shallowest depth; 8 cm) of Pedon 2, decrease with depth, and slightly increase again at the bottom of the profile (Table 3). A similar pattern is observed in Pedon 6, although the concentrations are not as high as in Pedon 2 and the patterns

Table 3. Summary of Soil Water Chemical Composition With Depth^a

	N	DIC	DOC	Na	K	Ca	Mg	Si	Fe	Al
<i>Pedon 2</i>										
8 cm	1	15	31		3	2,222	1,300	485	12.50	4.12
26 cm	1	91	885	111	7	457	96	254	1.80	1.00
39 cm	4	70 (44)	616 (642)	82 (25)	6 (3)	257 (105)	47 (21)	195 (118)	1.01 (0.66)	3.55 (3.95)
52 cm	2	88 (18)	932 (414)	91 (9)	7 (2)	262 (5)	47 (11)	338 (4)	0.87 (0.65)	8.39 (7.13)
76 cm	3	191 (198)	1022 (508)	156 (71)	8 (3)	678 (217)	94 (34)	273 (90)	1.31 (0.79)	2.77 (2.75)
<i>Pedon 5</i>										
25 cm	1		2125	19	33	234	42	150	0.64	1.47
59 cm	2	504	1951 (717)	429 (531)	29 (20)	258 (153)	124 (141)	381 (280)	0.71 (0.90)	4.69 (3.70)
101 cm	7	1666 (881)	2079 (627)	78 (47)	29 (13)	173 (77)	20 (4)	132 (68)	0.43 (0.40)	2.24 (2.36)
<i>Pedon 6</i>										
20 cm	1			7	81	299	42	175	0.67	1.92
51 cm	3		3190	86 (29)	71 (19)	161 (8)	43 (2)	156 (53)	0.27 (0.12)	5.74 (8.42)
71 cm	1		3541	71	60	96	22	222	0.18	0.41
84 cm	10		4570 (1207)	118 (30)	178 (277)	96 (11)	27 (3)	230 (56)	4.12 (12.27)	0.67 (0.74)

^aMean values (in micromoles L⁻¹) are shown with one standard deviation in parentheses.

are not as pronounced. Base cations (Na, Ca, Mg) are highest at middepths (59 cm) in Pedon 5. The anomalous enrichment of base cations in soil pore waters near the surface in Pedon 2 is consistent with the observed enrichment of Ca, Mg, and Sr in solid soil samples from that depth in Pedon 2. The highest Si concentration was observed at the shallowest depth in Pedon 2, middepth in Pedon 5, and deepest depth in Pedon 6, although a wide range of values were observed at each depth. DIC concentrations were the highest in the deepest depths in Pedons 2 and 5; there were no DIC data from Pedon 6 due to limited sample volume. DOC concentrations were relatively consistent with depth in Pedon 2 (except for the shallowest depth) and Pedon 5, and slightly increased with depth in Pedon 6. Iron concentrations were low in pore waters from all of the soil depths sampled, except for the shallowest depth in Pedon 2, and deepest depth (84 cm) in Pedon 6. Aluminum concentrations were highest at middepths in all three pedons. Chemical fluxes for Na and Si based on average soil water chemistry values and average cumulative annual water fluxes for all pedons (measured in WY 2011 and 2012) [Vázquez-Ortega *et al.*, 2015] were 14 (±7.5) and 31 (±6.7) mmol m⁻² yr⁻¹, respectively (Table 1); there were not enough paired solute chemistry and water flux measurements to compare solute fluxes across pedons.

3.4. Springs

Solute concentrations indicate that spring water sources can be divided into two unique categories that we refer to as “shallow groundwater” and “deep groundwater” (Table 2). High elevation springs (shallow groundwater) on Redondo Peak have similar Na, DIC, SO₄, and Cl concentrations as soil water, and represent shorter residence time and local water recharge sources. In contrast, low elevation springs near the base of Redondo Peak (Cowboy and Redondo Meadow springs) have higher total solute concentrations, lower DOC, and are enriched in Na and Si compared to soil water and high elevation springs. Water from these low elevation springs likely represents deeper groundwater, derived from longer flow paths and transit times, and larger contributing areas through Redondo Peak [Zapata-Rios *et al.*, 2015b]. There are no springs visible within the low elevation parts of La Jara catchment, where the stream drains into a broad, alluvial fan. Thus, inclusion of these low elevation springs at the base of Redondo Peak, but outside La Jara catchment, enables sampling of representative deeper/longer residence time groundwater that may be contributing to La Jara Creek.

Redondo Meadow and Cowboy springs have perennial discharge that does not respond to precipitation events (snowmelt or summer monsoons), maintains temporally consistent solute concentrations, and exhibits longer transit time (approximately 14 years for Redondo Meadow spring, based on tritium analysis) compared to high elevation springs [Zapata-Rios *et al.*, 2015b]. Shallow and deep groundwater from high and low elevation springs, respectively, have low DOC concentrations compared to soil water (Table 2). Aluminum, Fe, and Mn concentrations in Redondo Meadow and Cowboy springs (deeper groundwater) were all lower than concentrations in higher elevation springs discharging into La Jara Creek (representing shallow groundwater). Shallow groundwater Al, Fe, and Mn concentrations were lower on average than soil waters. Ge concentrations for the high elevation springs (shallow groundwater) that were analyzed ranged from 72

to 482 pmol L^{-1} (287 pmol L^{-1} average; Table 2); Ge concentrations were not measured for deep groundwater. Combining these results with Si concentrations, Ge/Si ratios ranged from 0.13 to $1.89 \text{ } \mu\text{mol mol}^{-1}$. Springs were not sampled as part of this study at high enough temporal resolution to observe any trends in Ge/Si ratios over time or with fluctuations in the hydrograph as observed with the stream waters. Spring waters are undersaturated with respect to albite, sanidine, calcite, and gypsum, but saturated with respect to secondary minerals gibbsite, goethite, hematite, and kaolinite, which should tend to precipitate along hydrologic flow paths based on the results of NETPATH modeling [Zapata-Rios *et al.*, 2015b].

3.5. Surface Waters

La Jara stream water chemistry exhibited inter and intra annual variability, presumably associated with changes in flow path and source water contributions, driven by substantial variations in precipitation and stream discharge among the four WYs and with season (Figure 7a). DOC concentrations were highest during peak snowmelt in WYs 2010 and 2012 (Figure 7b), and lower in WY 2011 and 2013. DOC and Al concentrations in surface waters draining the ZOB (in WY 2010) were higher than La Jara Creek and more similar to soil waters (Table 2). WY 2010 was a relatively wet year with a thick and consistent snowpack. Discharge increased by at least one order of magnitude starting in early April and was elevated for about 2 months. Peaks in discharge during spring snowmelt were also seen in WYs 2012 and 2013, although lower in magnitude compared to WY 2010. WY 2011 had a relatively dry winter, with a short snow season and thin snowpack, which allowed for soil freezing. Little snowmelt infiltration and stream flow response were seen during WY 2011 spring snowmelt.

A peak in La Jara stream water DOC was also observed during the summer North American Monsoon (NAM) in WY 2011, which was relatively wet and led to a peak in stream discharge. Increases in DOC were not detected during the NAM in other water years (WY 2010 and 2012), which only had small to no detectable peaks in discharge (WY 2012 and 2010, respectively). DIC patterns, in general, are the opposite of DOC, with a slight decrease during spring snowmelt, and the highest concentrations observed during the summer monsoons (Figure 7b, also see *Perdrial et al.* [2014a]).

Calcium concentrations in La Jara Creek were highest at the beginning of spring snowmelt in WY 2011 and 2012, and in the middle of the snowmelt period in 2013, with an additional peak during the summer monsoon in WY 2012 (Figure 7c). There was little change in Ca, Mg, K, and Na concentrations in La Jara Creek during snowmelt in WY 2010, and surface waters from the ZOB flume contained higher base cation concentrations compared to La Jara Creek, more similar to soil waters (Table 2). Na, K, and Mg concentrations in La Jara Creek seemed to follow similar trends as Ca, with their peaks offset by a few weeks from Ca during snowmelt in 2012. Si concentrations also peaked during spring snowmelt, although there was little increase in WY 2013. Average Si concentrations in the ZOB surface waters during snowmelt (WY 2010) were most similar to shallow groundwater (Table 2).

Solute fluxes based on stream solute concentrations and discharge for the three water years ranged from 5 (± 0.1) to 15 (± 0.5) and 12 (± 0.1) to 38 (± 0.01) $\text{mmol m}^{-2} \text{ yr}^{-1}$, for Na and Si, respectively (Table 1). Sodium solute fluxes derived from soil water and La Jara stream water are within the same range, and slightly higher (although the same magnitude) than long-term Na weathering rates derived from depletion analysis of ZOB soils (Table 1). In contrast, Si fluxes derived from soil water and stream water, which are comparable to each other, are an order of magnitude lower than Si weathering rates from ZOB soils (Table 1).

Ge/Si ratios are particularly useful for tracing soil water inputs as soil waters have high Ge/Si ratios from dissolution of Ge-rich kaolinite [Lugolobi *et al.*, 2010; Kurtz *et al.*, 2011] and/or Ge complexation with dissolved organic matter [Pokrovski *et al.*, 1998a, 1998b, 2000]. Ge/Si ratios were highest at the beginning of spring snowmelt in WY 2010, and remained consistently low in WY 2011 (Figure 7d). Al concentrations were higher than Fe in stream flow throughout the year, except at the beginning of snowmelt in WY 2013, and the highest Al concentrations were observed during spring snowmelt (Figure 7e). Small increases in Al and Fe were also seen in the summer monsoon in WYs 2010–2013.

Base cations, Si, Al, Fe, DIC, DOC, and Ge/Si ratios vary as a function of discharge in La Jara Creek (Figure 8). On a log-log scale, as C-Q relationships are often displayed [e.g., Godsey *et al.*, 2009], DOC and Al increase significantly with discharge (p values < 0.0001), with the maximum concentrations equivalent to surface waters draining the ZOB during snowmelt (Figures 8a and 8d). In contrast, there was no significant

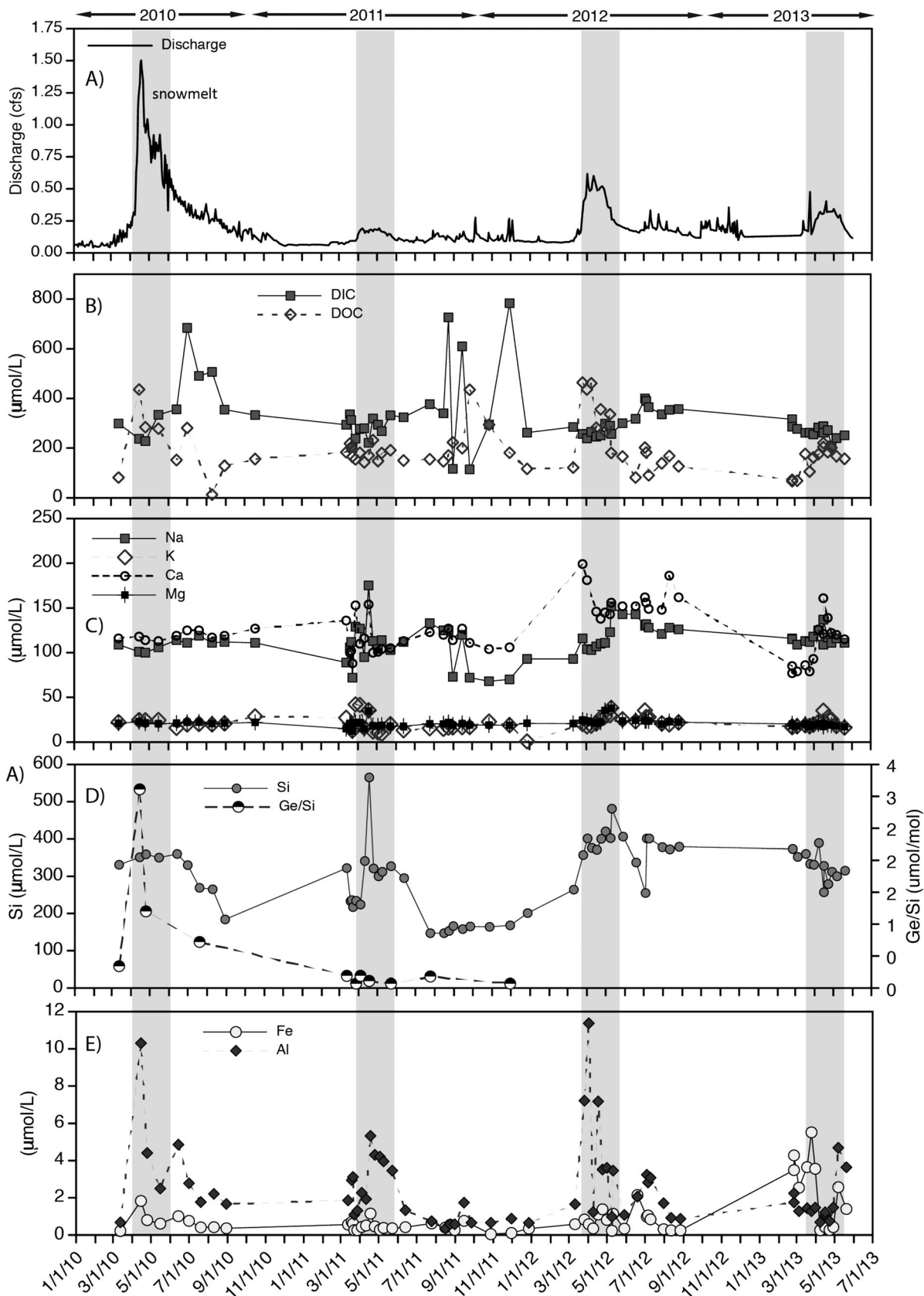


Figure 7. Time series of La Jara Creek discharge (daily) and chemistry (in micromoles L^{-1}), collected from the flume at the catchment outlet (Figure 1). Stream water samples were collected at higher-frequency (\sim weekly during spring snowmelt and summer monsoons) starting in 2011. The grey-shaded areas highlight the snowmelt season.

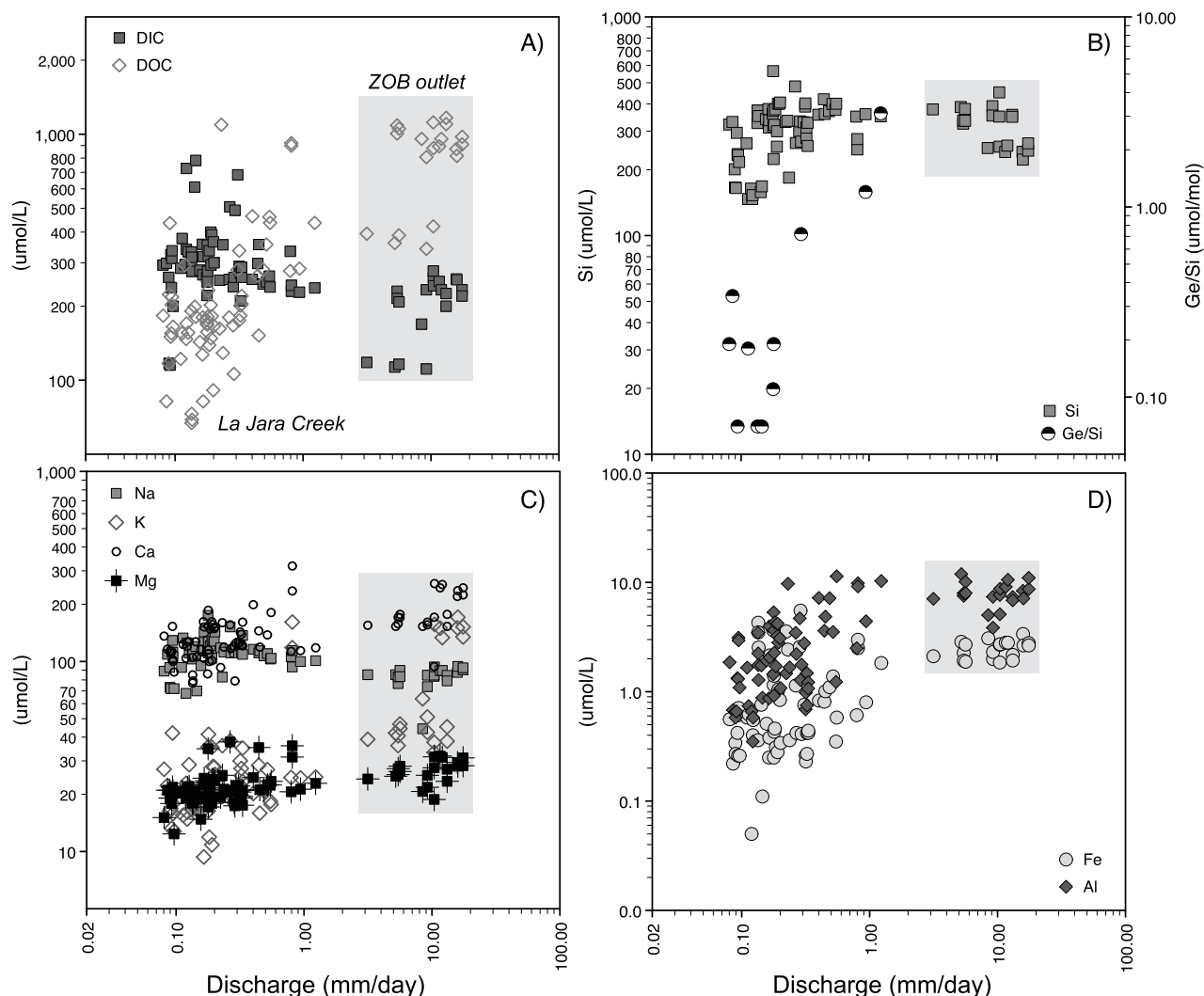


Figure 8. Concentration (in micromoles L^{-1}) versus discharge relationships for (a) dissolved inorganic and organic carbon, (b) Si and Ge/Si, (c) major cations, and (d) Fe and Al in La Jara Creek surface waters on log-log scale. Surface waters from a flume near the outlet of the ZOB, which drains into La Jara Creek, are included, and highlighted with the grey shading behind the symbols.

relationship between DIC, Si, Na, K, Ca, Mg, and discharge (Figures 8a–8c) with DIC, Na, K, Ca, and Mg concentrations exhibiting near-chemostatic behavior both in La Jara Creek and the ZOB outlet. Surprisingly, there was also no significant relationship between Fe and Mn with discharge, although Fe concentrations in the ZOB outlet during snowmelt are relatively high (within range of the highest stream water values). Si values are variable, especially at low discharge (Figure 8b). Ge concentrations and Ge/Si ratios were positively correlated with DOC concentration (r^2 values of 0.79 and 0.84, respectively; Figure 9a). There is a lot of variability in Al, Fe, and Mn concentrations with DOC, although the highest Al and Mn values are only seen at high DOC concentrations, and the highest Fe values are seen at the lowest DOC concentrations (Figure 9b). There was no significant relationship between base cations and DOC concentrations.

4. Discussion

Comparison of weathering rates from soil profiles, assumed to represent CZ development over thousands of years, to solute fluxes in soil and stream waters with relatively short transit times, reveals how biogeochemical processes and C-Q relationships may have evolved over variable timescales [White *et al.*, 2009]. In addition, understanding the sources of solutes (i.e., reactions and reservoirs within the CZ) and flow paths

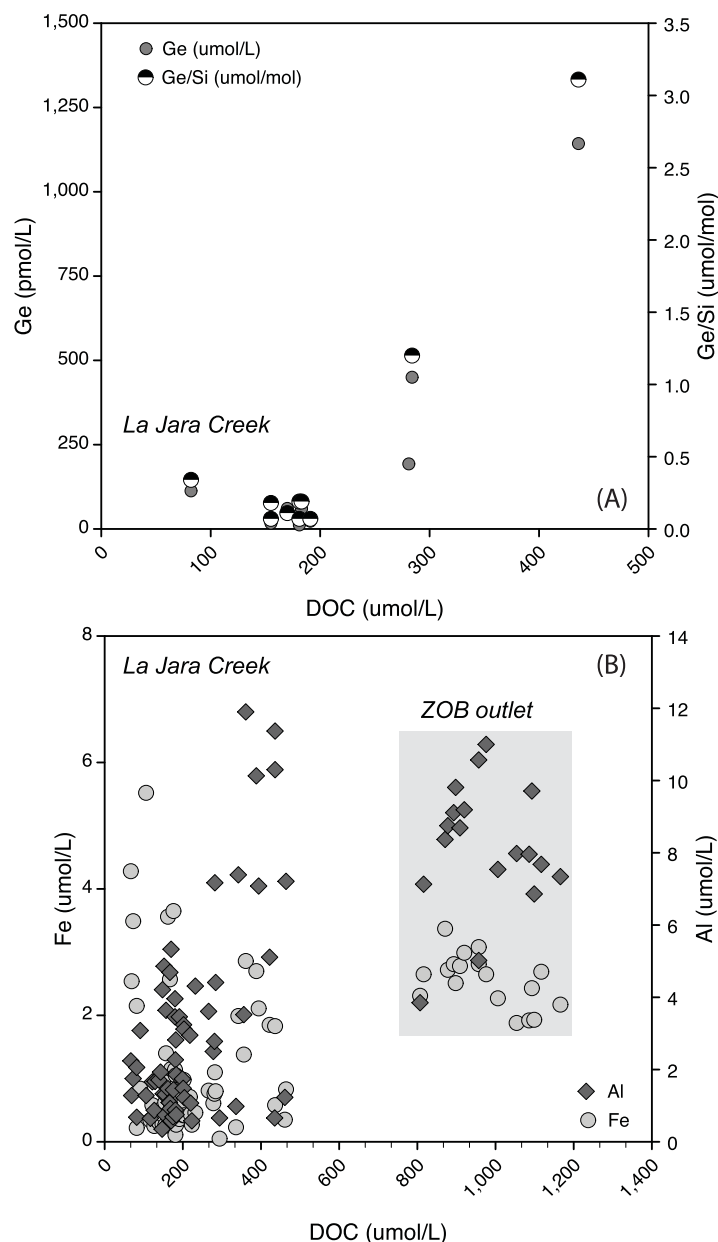


Figure 9. (a) Ge concentration (in picomoles L⁻¹) and Ge/Si ratios (in micromoles mol⁻¹), and (b) Fe and Al (in micromoles L⁻¹) compared to dissolved organic carbon (DOC) concentrations (in micromoles L⁻¹) in La Jara Creek waters. Surface waters from a flume near the outlet of the ZOB, which drains into La Jara Creek, are included, and highlighted with the grey shading behind the symbols.

to streamflow, and how they vary with hydrologic conditions helps to inform C-Q relationships [Godsey *et al.*, 2009; Stalard and Murphy, 2014].

4.1. Long-Term Evolution of CZ Structure

Previous studies have found differences in weathering rates and water fluxes (amount and timing) with landscape position in marine terraces in Santa Cruz, California [White *et al.*, 2008, 2009], and in the Santa Catalina, Boulder Creek, and Shale Hills Critical Zone Observatories (CZO), which can then influence solute fluxes to stream waters [Lin *et al.*, 2010; Anderson *et al.*, 2011; Lybrand *et al.*, 2011; Holleran *et al.*, 2015; Langston *et al.*, 2015]. We expected to see a similar positive relationship between shallow Na and Si weathering rates in soils and TWI, cumulative annual water fluxes, and landscape position in the La Jara ZOB. Previous studies found the highest REY depletion, organo-metal colloid complexation, and ²³⁴U enrichment at depth in Pedons 2 and 5, in the concave center of the La Jara ZOB, attributed to greater lateral subsurface fluxes of water and DOC [Vázquez-Ortega *et al.*, 2016; Huckle *et al.*, 2016]. However, we found no clear relationship between Na and Si weathering rates and TWI, cumulative water fluxes or landscape position in the ZOB, which may be due to differences in underlying bedrock geology and/or the shallow

depth of observation. In addition, TWI may not be a good indicator of deeper vadose zone water availability and distribution in semiarid to semihumid landscapes where water tables are deep (approximately 28–36 m on the NE and SW-facing hillslopes of the ZOB) [Moravec *et al.*, 2016] and evaporative demands are high compared to more humid climates.

Regolith depths in the ZOB (and adjacent catchments) based on recent geophysical survey and borehole drilling results range from 27 ± 4 m to 49 ± 10 m [Olyphant *et al.*, 2016; Moravec *et al.*, 2016]; the greatest depth to bedrock (thickest regolith) and likely highest bedrock weathering rates were seen on side slopes and ridge tops with the lowest TWI and deepest water table, while the shallowest depth to bedrock (thinnest regolith) and water table were seen in the valley bottom of the ZOB where TWI is the highest. The use

of the lowest soil horizon as the parent material in the chemical depletion and elemental weathering rate calculations likely underestimates the amount of weathering, especially in the tuff which is generally aphanitic with a large volcanic glass component that would increase its susceptibility to weathering.

Annual water balance and $EEMT_{TOPO}$ values for La Jara catchment and Redondo Dome are on the border between water and energy-limited systems [Rasmussen *et al.*, 2015]. North-facing slopes are generally energy limited, while south-facing slopes are generally more water-limited. Sodium weathering rates for soils in the ZOB, which has an overall south-facing aspect, are within the range of soils in other water-limited systems ($<0.08 \text{ mol m}^{-2} \text{ yr}^{-1}$) suggesting a consistent climate control on Na loss and plagioclase weathering across a range of systems [Rasmussen *et al.*, 2011]. In addition, the range and average values of Si weathering rates for soils in the La Jara ZOB are consistent with Si mass loss from a mixed conifer system on rhyolitic tuff in the Chiricahua Mountains of southeastern Arizona with a similar climate and parent material composition [Heckman and Rasmussen, 2011].

The estimates of soil age we obtained (16.5–25 ka) for the ZOB correspond to the Late Pleistocene, which was wetter and colder than current Holocene conditions [e.g., Thompson *et al.*, 1993]. The study site was likely above treeline at the Last Glacial Maximum, similar to other high-elevation sites around the region [Weng and Jackson, 1999]. In the absence of mature vegetation, rates of soil production were likely relatively low at that time. As such, even though the ZOB soils may have been subjected to a different climate, it is reasonable to expect that soil development would have been dominated by Holocene climatic conditions. More broadly, it is also reasonable to expect that effects of increased water availability and decreased temperature would have been partially offsetting. That is, greater water availability can be expected to increase weathering rates, but colder temperatures likely led to a decrease in weathering rates.

The marked enrichment in Mn in the O-horizon of ZOB soils (Figure 5) can be explained by dust deposition, as dust in the study area (and many other locations) [Herndon *et al.*, 2011] is enriched in Mn. Snow samples in the ZOB are also enriched in Mn compared to the other water types, likely from dust deposition. The enrichment of Ca, Mg, and Sr at the top of the soil profiles (Figure 4) is likely from decomposition of organic matter accumulated in the O-horizon [Likens *et al.*, 1998; Jobbagy and Jackson, 2004; Reich *et al.*, 2005; Berger *et al.*, 2006; Herndon *et al.*, 2015], as dust in the study area is depleted in these divalent cations. There is no enrichment in Na, K, or Si in the O-horizon, and dust in the study area is depleted in these elements, thus we assume that Na and Si are primarily rock derived. Ge is slightly less depleted than Si with depth in shallow soils (Figure 6), as Ge is more likely to precipitate with secondary minerals [Derry *et al.*, 2006].

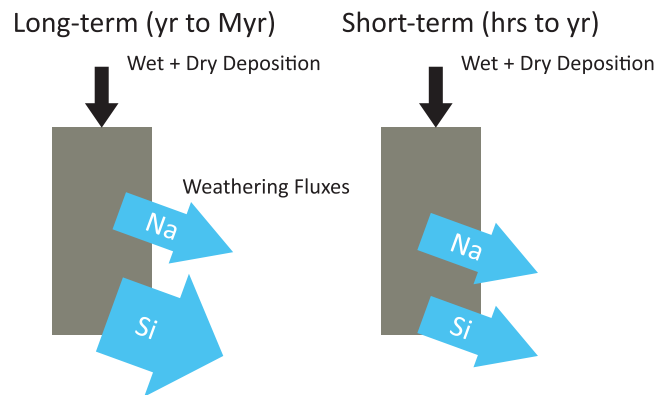
4.2. Geochemical Evolution of Waters Through the CZ

Understanding how the geochemistry of water varies and evolves through the heterogeneous CZ structure helps to constrain processes controlling stream flow C-Q relationships [Frisbee *et al.*, 2013]. Soil waters, shallow and deep groundwater, and surface water sampled within the La Jara catchment CZ have similar pH values and major cation chemistry (Table 2), dominated by Ca, Na, and Si, which suggests a similar source of solutes and rock-buffering, likely from dissolution of plagioclase feldspars. K-feldspars were observed in the soils, however plagioclase is more reactive and is therefore more likely to dominate stream water chemistry [Probst *et al.*, 2000; White *et al.*, 2001, 2008; Maher *et al.*, 2009; Moore *et al.*, 2012].

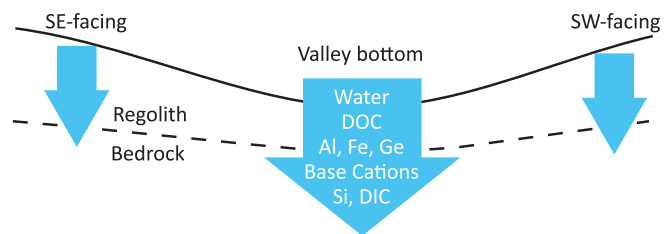
Soil waters have the highest average concentrations of DOC, Ca, Mg, Sr, Fe, and Al among the water types (Table 2), likely from evaporation, biologic inputs (e.g., degradation of organic matter) and cycling [Herndon *et al.*, 2015], and polyvalent cation complexation with organic matter. Enrichment of Na, Ca, Mg, DOC, and Fe in soil pore waters at the shallowest depth (O-horizon) in Pedon 2 (Table 3) is consistent with the elevated concentrations observed in solid soil samples (Figures 4 and 5), and can be attributed to decay of organic matter and colloid formation [Oades, 1988]. Microbial processing of DOC can account for the decrease in concentration between soil water, shallow groundwater, and deeper groundwater [Miller and Zepp, 1995]. The lack of a discernible pattern in soil pore water chemistry with landscape position or underlying bedrock geology is consistent with the solid phase soil results, although only three of the six pedons produced enough soil water to compare across the ZOB.

Shallow and deep groundwater are enriched on average in Na, Si, and DIC compared to soil water, surface water, and precipitation. The increase in Na and Si concentrations in groundwater with depth (highest value observed in the lowest elevation spring, Cowboy Spring) suggests increased plagioclase weathering along

A) Pedon-scale



B) Zero Order Basin (ZOB)-scale



C) Catchment-scale

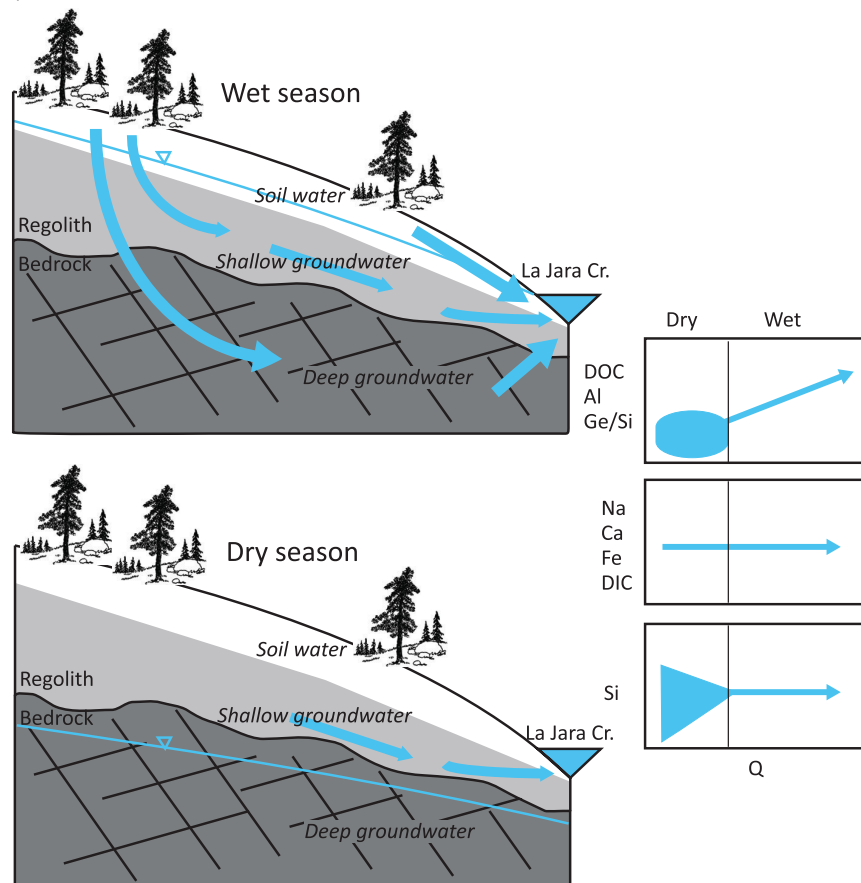


Figure 10.

deeper flow paths with increasing water residence time [Uchida *et al.*, 2003, Frisbee *et al.*, 2013]. The increase in Na and Si with depth also supports the hypothesis that deeper weathering profiles and reaction fronts exist in the underlying regolith in the ZOB, deeper than what is measured in the relatively shallow ZOB soil profiles, as was also observed, e.g., in more humid CZOs [Brantley *et al.*, 2013; Buss *et al.*, 2013; Kim *et al.*, 2014]. The recent deep borehole excavations and geophysical surveys in the ZOB support this contention, and indicate visible silicate mineral weathering fronts, and thick regolith that extend to more than 40 m in depth [Olyphant *et al.*, 2016; Moravec *et al.*, 2016].

Deep weathering zones in the Luquillo CZO extend lower than the stream channel in headwater catchments, suggesting a flux of solutes along deeper flow paths than observed in the headwater streams [Buss *et al.*, 2013]. Our results are consistent with this conceptual model, as the Na and Si concentrations in La Jara stream water are similar to the maximum values observed in soil pore waters and slightly lower than shallow groundwater, while groundwater discharging at low elevations in the VCNP (Cowboy Springs) have higher Na and Si concentrations indicating the plagioclase weathering zone may be deeper than the base of La Jara Creek. The lower $^{234}\text{U}/^{238}\text{U}$ activity ratios downstream in La Jara Creek suggest increasing contributions of deeper groundwater at lower elevation [Huckle *et al.*, 2016]. Several authors have pointed out that shallow springs, such as the high elevation ones on Redondo Dome, likely contain a mixture of waters with variable transit times and flow paths [e.g., Manga, 2001; Frisbee *et al.*, 2011, 2012, 2013].

4.3. Comparison of Long and Short-Term CZ Development and Solute Fluxes

The higher Si flux from the CZ over geologic timescales compared to more recent fluxes of mineral weathering-derived solutes (Table 1 and Figure 10a), suggests that dissolved Si released from dissolution of primary minerals likely precipitates as secondary minerals (e.g., layer silicate clays) in deeper regolith and fractured bedrock along flow paths to the stream. Stream waters are supersaturated with respect to amorphous silica and clays (e.g., kaolinite) [Zapata-Rios *et al.*, 2015b]. This supersaturation suggests there is a sink for Si in the CZ, likely from precipitation of clays, and thus Si is not transported conservatively to the stream. On the other hand, the similarity in Na weathering rates from soils and Na solute fluxes in soil water and stream water suggests that Na behaves relatively conservatively and is a good indicator of the extent of weathering and water residence time [Zapata-Rios *et al.*, 2015b].

The similar values for Na and Si solute fluxes derived from soil water and stream water also suggest that albite (Na-rich plagioclase) is a dominant primary mineral controlling solute chemistry and that Si has been removed from solution via secondary mineral precipitation (i.e., incongruent dissolution of plagioclase), as the $\sim 1:2$ Na:Si molar ratio is higher than that of albite's stoichiometry (1:3 Na:Si). This same incongruent reaction produces clays with high Ge/Si ($\sim 4\text{--}5$), and residual water with lower Ge/Si (~ 0.3 or less), depending on the mass balances. The low Ge/Si observed in base flow stream samples (averaging near $0.2 \text{ pmol } \mu\text{mol}^{-1}$), relative to fresh bedrock ($2.0 \text{ pmol } \mu\text{mol}^{-1}$ average), is consistent with the precipitation of secondary alumino-silicate phases along flow paths to the stream [Lugolobi *et al.*, 2010]. Ge/Si ratios in shallow groundwater and snowmelt stream samples are somewhat higher, with values near $0.9 \text{ pmol } \mu\text{mol}^{-1}$. These values may imply: (a) more "congruent" dissolution of primary silicates, i.e., lower rates of secondary phase formation, or (b) partial dissolution of clays in shallow soils that will have elevated Ge/Si.

Furthermore, the similarity in Na fluxes between soils, soil water, and stream water suggests that silicate mineral weathering at the catchment scale in La Jara is primarily controlled by water flux [Maher, 2010]. Thus, with increasing soil wetting and stream discharge during spring snowmelt we would expect to see

Figure 10. Conceptual model of CZ development, flow paths, and solute fluxes controlling C/Q relationships across temporal and spatial scales. (a) Comparable Na weathering rates from soils (long, geologic timescales) and Na solute fluxes from soil waters and stream waters (shorter, modern timescales) suggest that wetting of soil, regolith, and bedrock surfaces during spring snowmelt (in relatively wet years) promotes primary mineral dissolution and provides a constant supply of base cations and DIC to soil water and groundwater, only limited by the water flux. In contrast, higher Si weathering rates over geologic timescales versus recent Si fluxes, combined with solute chemistry and Ge/Si ratios suggests that interaction with secondary clay minerals controls Si/Q relationships in soil waters and stream flow. (b) The highest base cation, Si, Al, and Ge (impacted by colloidal transport and organic matter complexation) and DIC fluxes are found in convergent areas (b) where water and DOC fluxes are the highest; flushing of these convergent zones during spring snowmelt controls C/Q relationships under high flow conditions. (c) Si and base cation concentrations remain constant despite increasing discharge likely due to flushing of rock-derived solutes from different reservoirs in the CZ and mixing in the near-stream environment. Under dry conditions, stream flow is primarily supplied by drainage of shallow perched aquifers, while the regional water table is likely below the level of the stream channel, and reaction with clay minerals in perched aquifers may lead to variable Si concentrations.

relatively constant Na concentrations in stream flow from a constant supply of rock-derived Na. The non-conservative transport of Si and precipitation of secondary clay minerals along flow paths likely leads to variable Si relationships with discharge.

Si fluxes in La Jara soil and stream water are lower than more humid volcanic catchments, which range from 100 to 10,000 mmol m⁻² yr⁻¹ (excluding any hydrothermal inputs) for the Lesser Antilles [Goldsmith *et al.*, 2010], Reunion Island [Louvat and Allègre, 1997], Martinique and Guadeloupe [Rad *et al.*, 2006], Iceland [Louvat *et al.*, 2008], the Philippines [Schopka *et al.*, 2011], New Zealand [Goldsmith *et al.*, 2008], and the Deccan Traps [Dessert *et al.*, 2001]. The lower Si fluxes in La Jara catchment can be attributed to the lower discharge in the subhumid study area as the dissolved Si concentrations are within the same range as these other regions, and within the same range as the average maximum Si concentration of rivers draining basaltic terrains in the United States and Iceland (324 $\mu\text{mol L}^{-1}$) [Ibarra *et al.*, 2016].

4.4. Seasonal and Interannual Changes in Solute Fluxes and Controls on C-Q Relationships

Short-term fluxes of mineral weathering and biologically derived products of CZ development, and seasonal or interannual variations in stream water chemistry and C-Q relationships can inform how weathering reactions, source water contributions, and flow paths to stream discharge vary with climate [Church, 1997; Rademacher *et al.*, 2005; Godsey *et al.*, 2009; Steefel and Maher, 2009; Maher, 2010, 2011]. Several different patterns were observed in the C-Q relationships for La Jara Creek streamflow across WYs: (1) DIC and base cations are relatively constant; (2) Si values are more variable with discharge, except under the highest flow conditions ($>0.79 \text{ mm d}^{-1}$), which were only seen in the relatively “wet” winter of WY 2010; and (3) Al, DOC, and Ge/Si ratios are positively correlated with increasing discharge. There is no dilution trend in La Jara Creek streamflow C-Q relationships, further confirming the lack of direct overland flow to the stream in this subhumid climate, with well-drained soils.

The “chemostatic” behavior of Na, K, Ca, Mg, Sr, and DIC during high flow conditions, and the similar Na weathering rates from soils and solute fluxes from soil and stream waters (Table 1; Figure 10), may be explained by production and conservative transport of solutes derived from primary mineral weathering (e.g., plagioclase). Wetting of soil and regolith surfaces during spring snowmelt promotes primary mineral dissolution at chemical reaction rates that are faster than the advective mass transport rates (i.e., a high Damköhler number); [e.g., Maher and Chamberlain, 2014]. This provides a constant supply of base cations and DIC to soil water and groundwater, only limited by the water flux—similar to the model proposed by Godsey *et al.* [2009] to explain C-Q relationships in streamflow. Because soil water, ZOB surface water, and shallow groundwater have similar base cation and DIC concentrations, and are well mixed in convergent areas (e.g., ZOB swale) and the near-stream environment during “wet” periods (Figure 10b), the chemical composition of the stream remains relatively constant with increasing discharge. This explanation is similar to the reservoir-based end member mixing model approach used by other researchers to explain C-Q relationships [Hooper *et al.*, 1990; Anderson *et al.*, 1997]. In addition, draining of shallow groundwater from perched aquifers or interflow zones likely sustains La Jara Creek base flow during “drier” periods when the water table (i.e., deeper groundwater) is disconnected from the stream (Figure 10c), as the Na, Si, and DIC concentrations in stream flow most closely resemble shallow groundwater throughout the four WYs.

Si versus discharge relationships are more variable than base cations and DIC, likely because Si is not transported conservatively to the stream as a result of precipitation of aluminosilicate clays. These results are consistent with previous studies pointing out the importance of secondary mineral precipitation controlling Si fluxes [Godsey *et al.*, 2009; Maher, 2011]. Under low flow conditions, interaction of shallow groundwater with clays in perched aquifers likely leads to variable Si concentrations that never reach values as high as deep groundwater. Under high flow conditions, only observed in the wettest WY (2010), snowmelt infiltration may raise the water table, pushing up deeper groundwater derived from previous years snowmelt, which mixes with soil water and shallow groundwater in the near stream environment, as well as drainage from convergent upland areas, leading to higher and relatively “constant” Si concentrations in stream waters at the highest discharge (Figure 10c). The lack of elevated Si concentrations in La Jara Creek during snowmelt in WY 2010, when we expected the greatest infiltration and contribution of deep groundwater, may be due to inadequate (too low) resolution of sampling compared to subsequent snowmelt seasons

(i.e., we may have not sampled during the high Si pulse). This points to the need for higher resolution sampling of streamflow during the rising limb of the hydrograph in relatively “wet” snowmelt seasons. Higher variability in stream water base cation and Si concentrations observed in WYs 2011–2013 can be attributed in part to higher-resolution sampling, compared to WY 2010.

Some soil-derived solutes that are released from incongruent mineral weathering and are transported by complexation with organic matter (i.e., Ge, Al, Mn) and/or as colloids (i.e., Al) increase in concentration with discharge [Trostle *et al.*, 2016] (Figure 10c). These ions may be quickly mobilized to the stream during periods of snowmelt infiltration, soil saturation, and subsurface lateral connectivity either through perched aquifers above clay layers or at the regolith-bedrock interface. These results are consistent with previous studies in other perennial mountain catchments that have shown increased influence of soil waters on stream waters during snowmelt periods and heavy rains [Johnson *et al.*, 1969; Clow and Drever, 1996]. Clow *et al.* [1997] found that in Loch Vale, Colorado, waters infiltrating soils during snowmelt periods, released a soil water chemical signature to streams. Similarly, work in other Rocky Mountain and Sierra Nevada catchments indicated that dissolved nutrient and metal concentrations during snowmelt were due to the flushing of soil and subsurface solute reservoirs [Williams and Melack, 1991; Brooks *et al.*, 1999, 2005; Heuer *et al.*, 1999]. During dry periods, hillslopes and upland convergent areas are disconnected from the stream and stream waters in these catchments are dominated by groundwater discharge.

The positive relationship between Ge and Ge/Si ratios, and Al with DOC and discharge (Figures 8 and 9) could indicate that water fluxes and organic matter complexation play key roles in driving weathering reaction in the CZO soils [Povroski *et al.*, 1998a, 1998b, 2000]. Ge concentrations and Ge/Si ratios may also be elevated in soil waters due to dissolution of secondary aluminosilicates such as kaolinite, which contain high concentrations of Ge relative to primary silicates [Lugolobi *et al.*, 2010; Kurtz *et al.*, 2011]. If soil waters become undersaturated with respect to kaolinite or smectite during periods of high snowmelt infiltration (e.g., WY 2010), the clays may dissolve to form gibbsite, releasing high Ge/Si and Al to solution; DOC complexation of Ge and colloid formation with Al may further enhance clay mineral dissolution and transport of metals to the stream [Derry *et al.*, 2006]. In addition, these results demonstrate the importance of biology (in terms of DOC) in regulating metal (e.g., Al) fluxes on an annual basis, and the role of convergent areas (swales) in controlling C-Q relationships for metals and elements associated with organic-rich soils during high flow conditions, consistent with the findings of Herndon *et al.* [2015] for shale headwater catchments.

Interestingly, soil freezing during WY 2011, due to an intermittent snowpack, limited snowmelt water infiltration and flushing of DOC, Al, Fe, and Ge from soils and convergent zones (e.g., ZOB outlet). The lack of a significant relationship between Fe and DOC, and Fe and discharge, may be due to the lower Fe concentrations in soil and surface waters compared to Al, preferential retention of Fe along subsurface flow paths, and/or the paucity of high-resolution sampling across the rise of the snowmelt hydrograph.

Together, the C-Q results support previous conceptual models for streamflow that suggest very little snowmelt runs off directly into La Jara Creek [Lyon *et al.*, 2008; Liu *et al.*, 2008a; Perdril *et al.*, 2014a]; rather, the majority of snowmelt infiltrates and resides in the CZ subsurface for a period of time (at least ~12 years according to tritium-based transit times of spring waters) [Zapata-Rios *et al.*, 2015b], reacting with soils, regolith and bedrock, before discharging to the stream in subsequent years [Kostrzewski, 2006; Liu *et al.*, 2008a, 2008b]. Even surface waters draining the ZOB swale during snowmelt are derived from soil and shallow groundwater (based on their similar chemistries), rather than overland flow. Shallow groundwater may exist as perched aquifers in the regolith associated with clay layers or at the bedrock-soil interface that may be slowly draining from snowmelt recharge, and discharge laterally to the ZOB swale and La Jara Creek, as the isotopic composition of shallow groundwater and stream water represent snowmelt throughout the year [Liu *et al.*, 2008a; Zapata-Rios *et al.*, 2015b] (Figure 10c). Deeper groundwater, possibly from the water table in the fractured bedrock, may be disconnected from the stream (i.e., deeper than La Jara Creek), except following relatively “wet” winters when deep percolation of snowmelt leads to substantial rises in the water table. Greater soil flushing during spring snowmelt in WY 2010 and 2012 may be attributed to more consistent snowpacks, unfrozen soils, and greater snowmelt infiltration from “wetter” winters, leading to rising shallow water tables, and subsurface lateral flow paths that intersect organic-rich soil horizons near the stream and mobilize DOC, Fe, Mn, Al, Ge, and REY [Perdril *et al.*, 2014a; Vázquez-Ortega *et al.*, 2015].

5. Summary

A multimethod approach that combined distributed data sets on chemistry of the weathering profile and multiple CZ water sources was needed to unravel mechanisms underlying C-Q relations in the La Jara catchment. Processes of solute production and retention in the CZ, over short and long-timescales are strongly impacted by groundwater fluxes and incongruent silicate mineral dissolution. Water in these reservoirs is displaced during the annual flushing of organic matter, colloids, and associated solutes that occurs during snowmelt. Export of these products of CZ development to streams is dependent on interannual and topographic variation in climate, water flux, and CZ structure. Comparable Na weathering rates over long-timescales with shorter-term Na solute fluxes provides evidence that silicate mineral weathering is primarily controlled by water fluxes in the subhumid JRB-CZO. Because soil water and shallow groundwater have similar base cation and DIC concentrations, and are mixed with deeper groundwater in the near-stream environment and runoff from convergent zones during “wet” periods, the chemical composition of the stream remains relatively constant (“chemostatic”) with increasing discharge.

Soil chemical depletion profiles, regolith thickness, and groundwater chemistry indicate that deep CZ weathering and release of Si and base cations from the highly fractured, young volcanic bedrock, is an essential contributor to stream chemical fluxes. Three lines of evidence indicate that Si is retained in secondary clay minerals along subsurface flow paths: (1) the observation of higher Si weathering rates from soils over geologic timescales relative to modern soil water and stream Si solute fluxes; (2) low Ge/Si ratios in stream base flow relative to fresh bedrock; and (3) supersaturation of stream waters with respect to amorphous silica and clays (e.g., kaolinite). Variability in Si concentrations at low Q may be explained by dissolution and precipitation of clays in perched aquifers. Lower Si fluxes in the subhumid La Jara Creek catchment, compared to streams in more humid volcanic terrains, can be attributed to lower water fluxes in the JRB-CZO, because Si concentrations are comparable to other sites.

During relatively “wet” winters, snowmelt infiltration likely causes a rise in the water table, flushing deeper groundwater derived from previous years snowmelt into the stream, leading to higher Q and higher, relatively constant Si concentrations in stream waters. During low-Q conditions, Si concentrations in stream waters never reach high levels seen in deeper groundwater, likely because the water table is disconnected from the stream (i.e., below stream base level), and draining of perched waters sustains base flow. Metals likely transported by complexation with organic matter (i.e., Ge, Fe, Al, Mn) and/or as colloids (i.e., Al, Fe) increase with increasing discharge, as soils are saturated during “wet” periods (e.g., spring snowmelt and summer monsoons) and hillslopes (via subsurface flow paths) and convergent areas drain to the stream. During periods of soil saturation, pore waters may become undersaturated with respect to layer silicate clays. Their dissolution and gibbsite precipitation may elevate the Ge/Si ratio and release Al to solution. DOC complexation of Ge and Al, and Al colloid formation may further enhance clay mineral dissolution and transport of metals to the stream. Higher-resolution sampling of C-Q relationships during the rising limb of the hydrograph and better characterization of groundwater dynamics (both in seasonally saturated regolith and fractured bedrock) will help to better constrain processes controlling the sources and fluxes of solutes through the CZ.

Acknowledgments

Funding for this project was provided by the Catalina-Jemez Critical Zone Observatory (NSF EAR-0724958; EAR-1331408). Additional funding was provided by a Geological Society of America Student Research Grant to C. Porter (now C. Schaumberg). We thank Mary Kay Amistadi, Tim Corley, David Huckle, James Ray, David Bernard, Claire Tritz, Aidan Io Blum, David Renner, and Lauren Koch for assistance with lab analyses and fieldwork. Matej Durcik generated the GIS map figures and helped with data management. We appreciate comments by Sue Brantley and two anonymous reviewers that greatly improved the manuscript. Data used in the study can be obtained from the IEDA database (<https://doi.org/10.1594/IEDA/100638>; <https://doi.org/10.1594/IEDA/100639>), and Hydroshare (<https://doi.org/10.4211/hs.28639de860f74340a3549735abb7b0c6>).

References

- Anderson, S. P., W. E. Dietrich, R. Torres, D. R. Montgomery, and K. Loague (1997), Concentration-discharge relationships in runoff from a steep, unchanneled catchment, *Water Resour. Res.*, 33(1), 211–225, doi:10.1029/96WR02715.
- Anderson, S. P., R. S. Anderson, E. L. S. Hincley, P. Kelly, and A. Blum (2011), Exploring weathering and regolith transport controls on critical zone development with models and natural experiments, *Appl. Geochem.*, 26, S3–S5.
- Arslan, Z., N. Ertas, J. F. Tyson, P. C. Uden, and E. R. Denoyer (2000), Determination of trace elements in marine phytoplankton by inductively coupled plasma mass spectrometry (ICP-MS), *Fresenius J. Anal. Chem.*, 366, 273–282.
- Bales, R. C., N. P. Molotch, T. H. Painter, M. D. Dettinger, R. Rice, and J. Dozier (2006), Mountain hydrology of the western United States, *Water Resour. Res.*, 42, W08432, doi:10.1029/2005WR004387.
- Berger, T.W., S. Swoboda, T. Prohaska, and G. Glatzel (2006), The role of calcium uptake from deep soils for spruce (*Picea abies*), *For. Ecol. Manage.*, 229, 234–246.
- Biederman, J. A., T. Meixner, A. A. Harpold, D. E. Reed, E. D. Gutmann, J. A. Gaun, and P. D. Brooks (2016), Riparian zones attenuate nitrogen loss following bark beetle-induced lodge pole pine mortality, *J. Geophys. Res. Biogeosci.*, 121, 933–948, doi:10.1002/2015JG003284.
- Bishop, K., J. Seibert, S. Köhler, and H. Laudon (2004), Resolving the Double Paradox of rapidly mobilized old water with highly variable responses in runoff chemistry, *Hydrol. Processes*, 18, 185–189, doi:10.1002/hyp.5209.
- Blecker, S. W., S. L. King, L. A. Derry, O. A. Chadwick, J. A. Ippolito, E. F. Kelly (2007), The ratio of germanium to silicon in plant phytoliths: Quantification of biological discrimination under controlled experimental conditions, *Biogeochemistry*, 86, 189–199.

- Boyer, E. W., G. M. Hornberger, K. E. Bencala, and D. M. McKnight (1997), Response characteristics of DOC flushing in an alpine catchment, *Hydrol. Processes*, *11*(12), 1635–1647.
- Brantley, S. L., M. B. Goldhaber, and K. V. Ragnarsdottir (2007), Crossing disciplines and scales to understand the critical zone, *Elements*, *3*(5), 307–314.
- Brantley, S. L., M. E. Holleran, L. X. Jin, and E. Bazilevskaya (2013), Probing deep weathering in the Shale Hills Critical Zone Observatory, Pennsylvania (USA): The hypothesis of nested chemical reaction fronts in the subsurface, *Earth Surf. Processes Landforms*, *38*, 1280–1298.
- Brantley, S. L., M. I. Lebedeva, V. N. Balashov, K. Singha, P. L. Sullivan, and G. Stinchcomb (2017), Toward a conceptual model relating chemical reaction fronts to water flow paths in hills, *Geomorphology*, *277*, 100–117.
- Brimhall, G. H., and W. E. Dietrich (1987), Constitutive mass balance relations between chemical composition, volume, density, porosity, and strain in metasomatic hydrochemical systems: Results on weathering and pedogenesis, *Geochim. Cosmochim. Acta*, *51*(3), 567–587.
- Brooks, P. D., and M. M. Lemon (2007), Spatial variability in dissolved organic matter and inorganic nitrogen concentrations in a Semi-arid Stream, San Pedro River, Arizona, *J. Geophys. Res.*, *112*, G03S05, doi:10.1029/2006JG000262.
- Brooks, P. D., and E. R. Vivoni, (2008), Mountain ecodrology: Quantifying the role of vegetation in the water balance of montane catchments, *Ecohydrology*, *1*, 187–192.
- Brooks, P. D., D. M. McKnight, and K. E. Bencala (1999), The relationship between soil heterotrophic activity, soil dissolved organic carbon (DOC) leachate, and catchment-scale DOC export in headwater catchments, *Water Resour. Res.*, *35*(6), 1895–1902.
- Brooks, P. D., D.M. McKnight, N.E. Driver and K.E. Bencala (2001), Annual maxima in Zn concentrations during spring snowmelt, *Environ. Geol.*, *40*, 1447–1454.
- Brooks, P. D., C. M. O'Reilly, S. A. Diamond, D. H. Campbell, R. Knapp, D. Bradford, P. S. Corn, B. Hossack, and K. Tonnessen (2005), Spatial and temporal variability in the amount and source of dissolved organic carbon: Implications for ultraviolet exposure in amphibian habitats, *Ecosystems*, *8*(5), 478–487.
- Brooks, P. D., J. Chorover, Y. Fan, S. E. Godsey, R. M. Maxwell, J. P. McNamara, and C. Tague (2015), Hydrological partitioning in the critical zone: Recent advances and opportunities for developing transferable understanding of water cycle dynamics, *Water Resour. Res.*, *51*, 6973–6987, doi:10.1002/2015WR017039.
- Broxton, P. D., P. A. Troch, and S. W. Lyon (2009), On the role of aspect to quantify water transit times in small mountainous catchments, *Water Resour. Res.*, *45*, W08427, doi:10.1029/2008WR007438.
- Burns, M. A., H. R. Barnard, R. S. Gabor, D. M. McKnight, and P. D. Brooks (2016), Dissolved organic matter transport and transformation reflects hillslope to stream connectivity during snowmelt in a semi-arid catchment, *Water Resour. Res.*, *52*, 4905–4923, doi:10.1002/2015WR017878.
- Buss, H. L., S. L. Brantley, F. N. Scatena, E. A. Bazilevskaya, A. Blum, M. Schulz, R. Jimenez, A. F. White, G. Rother, and D. Cole (2013), Probing the deep critical zone beneath the Luquillo Experimental Forest, Puerto Rico, *Earth Surf. Processes Landforms*, *38*(10), 1170–1186.
- Chadwick, O. A., G. H. Brimhall, and D. M. Hendricks (1990), From a black to a gray box: A mass balance interpretation of pedogenesis, *Geomorphology*, *3*(3), 369–390.
- Chanat, J. G., K. C. Rice, and G. M. Hornberger (2002), Consistency of patterns in concentration-discharge plots, *Water Resour. Res.*, *38*(8), 1147, doi:10.102912001WR000971.
- Chorover, J. (2012), Impact of soil physicochemical and biological reactions on transport of nutrients and pollutants in the critical zone, in *Handbook of Soil Science: Resource Management and Environmental Impacts*, edited by P. M. Huang, 10–1 to 10–35, Academic, New York.
- Chorover, J., et al. (2011), How water, carbon, and energy drive critical zone evolution: The Jemez-Santa Catalina Critical Zone Observatory, *Vadose Zone J.*, *10*, 884–899, doi:10.2136/vzj2010.0132.
- Chorover, J., J. Perdril, J. McIntosh, P. Troch, M. K. Amistadi, M. Losleben, K. Condon, and S. A. Pedron (2017), *Jemez River Basin Soil Solution Chemistry 2011 (New Mexico, USA), Integrated Earth Data Applications (IEDA)*, doi:10.1594/IEDA/100639.
- Church, M. R. (1997), Hydrochemistry of forested catchments, *Annu. Rev. Earth Sci.*, *25*, 23–59.
- Clow, D. W., and J. I. Drever (1996), Weathering rates as a function of flow through alpine soil, *Chem. Geol.*, *132*, 131–141.
- Clow, D. W., M. A. Mast, T. D. Bullen, and J. T. Turk (1997), Strontium 87/strontium 86 as a Tracer of mineral weathering reactions and calcium sources in an alpine/subalpine watershed, Loch Vale, Colorado, *Water Resour. Res.*, *33*(6), 1335–1351.
- Derry, L. A., J. C. Pett-Ridge, A. C. Kurtz, and J. W. Troester (2006), Ge/Sr and ⁸⁷Sr/⁸⁶Sr tracers Of weathering reactions and hydrologic pathways in a tropical granitoid system, *J. Geochem. Explor.*, *88*, 271–274.
- Dessert, C., B. Dupré, L. M. François, J. Schott, J. Gaillardet, G. Chakrapani, and S. Bajpai (2001), Erosion of Deccan Traps determined by river geochemistry: Impact on the global climate and the ⁸⁷Sr/⁸⁶Sr ratio of seawater, *Earth Planet. Sc. Lett.*, *188*(3), 459–474.
- Efron, B. and C. Stein (1981), The Jackknife Estimate of Variance, *Ann. Stat.*, *9*, 586–596.
- Egli, M., and P. Fitze (2000), Formulation of pedologic mass balance based on immobile elements: A revision, *Soil Sci.*, *165*(5), 437–443.
- Evans, C., and T. D. Davies (1998), Causes of concentration/discharge hysteresis and its potential as a tool for the analysis of episode hydrochemistry, *Water Resour. Res.*, *34*(1), 129–137.
- Field, J. P., et al. (2015), Critical zone services: Expanding context, constraints, and currency beyond ecosystem services, *Vadose Zone J.*, *14*(1), 1–7. doi:10.2136/vzj2014.10.0142.
- Frisbee, M. D., F. M. Phillips, A. R. Campbell, F. Liu, and S. A. Sanchez (2011), Streamflow generation in a large, alpine watershed in the southern Rocky Mountains of Colorado: Is streamflow generation simply the aggregation of hillslope runoff responses?, *Water Resour. Res.*, *47*, W06512, doi:10.1029/2010WR009391.
- Frisbee, M. D., F. M. Phillips, G. S. Weissmann, P. D. Brooks, J. L. Wilson, A. R. Campbell, and F. Liu (2012), Unraveling the mysteries of the large watershed black box: Implications for the streamflow response to climate and landscape perturbations, *Geophys. Res. Lett.*, *39*, L01404, doi:10.1029/2011GL050416.
- Frisbee, M. D., F. M. Phillips, A. F. White, A. R. Campbell, and F. Liu (2013), Effect of Source integration on the geochemical fluxes from springs, *Appl. Geochem.*, *28*, 32–54, doi:https://doi.org/10.1016/j.apgeochem.2012.08.028.
- Gallo, E. L., K. A. Lohse, P. D. Brooks, J. E. T. McLain, J. McIntosh, and T. Meixner (2012), Influence of channel substrate type on storage and transport of urban storm runoff in an arid environment, *J. Hydrol.*, *470–471*, 98–110, doi:10.1016/j.jhydrol.2012.08.047.
- Gallo, E. L., P. D. Brooks, K. A. Lohse, and J. E. T. McLain (2013), Land cover controls on summer discharge and runoff solution chemistry of semi-arid urban catchments, *J. Hydrol.*, *485*, 37–53, doi:10.1016/j.jhydrol.2012.11.054.
- Goddéris, Y. and S. L. Brantley (2013), Earthcasting the future critical zone, *Elementa*, *1*(1), 000019.
- Godsey, S. E., J. W. Kirchner, and D. W. Clow (2009), Concentration-discharge relationships reflect chemostatic characteristics of US catchments, *Hydrol. Processes*, *23*, 1844–1864.
- Goff, F. (2009), *Valles Caldera: A Geologic History*, TWP America, Inc., Singapore.

- Goff, F., J. N. Gardner, S. L. Reneau, and C. J. Goff (2006b), Preliminary geologic map of the Redondo Peak quadrangle, Sandoval County, New Mexico, *Open File Geol. Map-111*, New Mexico Bureau of Geology and Mineral Resources. [Available at <http://geoinfo.nmt.edu/publications/maps/geologic/ofgm/details.cfm?Volume=111>.]
- Goff, F., S. L. Reneau, S. Lynch, C. J. Goff, J. N. Gardner, P. Drakos, and D. Katzman (2005), Preliminary geologic map of the Bland Quadrangle, Los Alamos and Sandoval Counties New Mexico, New Mexico Bureau of Geology and Mineral Resources, *Open File Dig. Geol. Map OF-GM 112*.
- Goff, F., S. L. Reneau, C. J. Goff, J. N. Gardner, P. G. Drakos, and D. Katzman (2006a), Geologic map of the Valle San Antonio quadrangle, Sandoval County, New Mexico, *Open File Geol. Map-132*, New Mexico Bureau of Geology and Mineral Resources. [Available at <http://geoinfo.nmt.edu/publications/maps/geologic/ofgm/details.cfm?Volume=132>.]
- Goldsmith, S. T., A. E. Carey, W. B. Lyons, and D. M. Hicks (2008), Geochemical fluxes and weathering of volcanic terrains on high standing islands: Taranaki and Manawatu-Wanganui regions of New Zealand, *Geochim. Cosmochim. Acta*, 72(9), 2248–2267.
- Goldsmith, S. T., A. E. Carey, B. M. Johnson, S. A. Welch, W. B. Lyons, W. H. McDowell, and J. S. Pigott (2010), Stream geochemistry, chemical weathering and CO₂ consumption potential of andesitic terrains, Dominica, Lesser Antilles, *Geochim. Cosmochim. Acta*, 74(1), 85–103.
- Grossman, R. B., and T. G. Reinsch (2002), Bulk density and linear extensibility, in *Methods of soil analysis: Part 4 Physical methods*, edited by J. M. Dane, and G. C. Topp, pp. 201–228, Soil Sci. Soc. of Am., Madison, Wis.
- Guo, Q., J. Pelletier, R. Parmenter, C. Allen, B. Judy, and M. Durcik (2010), *CZO Dataset: Jemez River Basin — LiDAR (2010) — Snow-off*. [Available at <http://criticalzone.org/catalina-jemez/data/dataset/2613/>.]
- Hall, S., S. Weintraub, D. Eiriksson, P. D. Brooks, M. Baker, G. Bowen, and D. Bowling (2016), Stream nitrogen inputs reflect groundwater across a snowmelt-dominated montane to urban watershed, *Environ. Sci. Technol.*, 50(3), 1137–1146, doi:10.1021/acs.est.5b04805.
- Harpold, A. A., et al. (2014), LiDAR-derived snowpack data sets from mixed conifer forests across the Western United States, *Water Resour. Res.*, 50, 2749–2755, doi:10.1002/2013WR013935.
- Heckman, K. and C. Rasmussen (2011), Lithologic controls on regolith weathering and mass flux in forested ecosystems of the southwestern USA, *Geoderma*, 164(3), 99–111.
- Heidbüchel, I., P. A. Troch, and S. W. Lyon (2013), Separating physical and meteorological controls of variable transit times in zero-order catchments, *Water Resour. Res.*, 49, 7644–7657, doi:10.1002/2012WR013149.
- Heimsath, A. M., W. E. Dietrich, K. Nishiizumi, and R. C. Finkel (2001), Stochastic processes of soil production and transport: Erosion rates, topographic variation and cosmogenic nuclides in the Oregon Coast Range, *Earth Surf. Processes Landforms*, 26, 531–552.
- Henderson, A. K., and B. N. Shuman (2010), Differing controls on river- and lake-water hydrogen and oxygen isotopic values in the western United States, *Hydrol. Processes*, 24(26), 3894–3906.
- Herndon, E. M., L. Jin, and S. L. Brantley (2011), Soils reveal widespread manganese enrichment from industrial inputs, *Environ. Sci. Technol.*, 45, 241–247.
- Herndon, E. M., A. L. Dere, P. L. Sullivan, D. Norris, B. Reynolds, and S. L. Brantley (2015), Landscape heterogeneity drives contrasting concentration-discharge relationships in shale headwater catchments, *Hydrol. Earth Syst. Sci.*, 19, 3333–3347.
- Heuer, K., P. D. Brooks, and K. A. Tonnesen (1999), Nitrogen dynamics in two high elevation catchments during spring snowmelt 1996, Rocky Mountains, Colorado, *Hydrol. Processes*, 13(14–15), 2203–2214.
- Holleran, M., M. Levi, and C. Rasmussen (2015), Quantifying soil and critical zone variability in a forested catchment through digital soil mapping, *Soil*, 1(1), 47–64.
- Hood, E., D. M. McKnight, and M. W. Williams (2003), Sources and chemical character of dissolved organic carbon across an alpine/subalpine ecotone, Green Lakes Valley, Colorado Front Range, United States, *Water Resour. Res.*, 39(7), 1188, doi:10.1029/2002WR001738.
- Hood, E., M. N. Gooseff, and S. L. Johnson (2006), Changes in the character of stream water dissolved organic carbon during flushing in three small watersheds, Oregon, *J. Geophys. Res.*, 111, GO1007, doi:10.1029/2005JG000082.
- Hooper, R. P., N. Christophersen, and N. E. Peters (1990), Modelling streamwater chemistry as a mixture of soil water end-members: An application to the Panola Mountain catchment, Georgia, USA, *J. Hydrol.*, 116(1–4), 321–343.
- Hornberger, G. M., K. E. Bencala, and D. M. McKnight (1994), Hydrological controls on dissolved organic carbon during snowmelt in the Snake River near Montezuma, Colorado, *Biogeochemistry*, 25(3), 147–165, doi:10.1007/BF00024390.
- Hornberger, G. M., T. M. Scanlon, and J. P. Raffensberger (2001), Modelling transport of dissolved silica in a forested headwater catchment: The effect of hydrological and chemical time scales on hysteresis in the concentration-discharge relationship, *Hydrol. Processes*, 15, 2029–2038.
- Huckle, D., L. Ma, J. McIntosh, A. Vázquez-Ortega, C. Rasmussen, and J. Chorover (2016), U-series isotopic signatures of soils and headwater streams in a semi-arid complex volcanic terrain, *Chem. Geol.*, 445, 68–83.
- Ibarra, D. E., J. K. Caves, S. Moon, D. L. Thomas, J. Hartmann, C. P. Chamberlain, and K. Maher (2016), Differential weathering of basaltic and granitic catchments from concentration-discharge relationships, *Geochim. Cosmochim. Acta*, 190, 265–293.
- Jobby, E. G., and R. B. Jackson (2004), The uplift of soil nutrients by plants: Biogeochemical consequences across scales, *Ecology*, 85(9), 2380–2389.
- Johnson, N. M., G. E. Likens, F. H. Borman, D. W. Fisher, and R. S. Pierce (1969), A working model for the variation in stream water chemistry at the Hubbard Brook Experimental Forest, New Hampshire, *Water Resour. Res.*, 5(6), 1353–1363.
- Johnson, T. M., and D. J. DePaolo (1994), Interpretation of isotopic data in groundwater-rock systems: Model development and application to Sr isotope data from Yucca Mountain, *Water Resour. Res.*, 30(5), 1571–1587.
- Jones, R. L., and G. B. Dreher (1996), Silicon, *Methods of Soil Analysis, Part 3: Chemical Methods*, SSSA Book Ser., vol. 5, Madison, Wis.
- Kim, H., J. K. B. Bishop, W. E. Dietrich, and I. Y. Fung (2014), Process dominance shift in solute chemistry as revealed by long-term high-frequency water chemistry observations of groundwater flowing through weathered argillite underlying a steep forested hillslope, *Geochim. Cosmochim. Acta*, 140, 1–19.
- Kostrzewski, J. M. (2006), Quantifying seasonal variations in water source and nutrient concentrations: A catchment comparison in Valles Caldera National Preserve, NM, USA, MS thesis, Dep. of Hydrol. and Water Resour., Univ. of Arizona, Tucson.
- Kurtz, A. C., L. A. Derry, and O. A. Chadwick (2002), Germanium-silicon fractionation in the weathering environment, *Geochim. Cosmochim. Acta*, 66, 1525–1537.
- Kurtz, A. C., F. Lugolobi, and G. Salvucci (2011), Germanium-silicon path tracer: Application to the Rio Icacos watershed, *Water Resour. Res.*, 47, W06516, doi:10.1029/2010WR009853.
- Langston, A. L., G. E. Tucker, R. S. Anderson, and S. P. Anderson (2015), Evidence for climatic and hillslope-aspect controls on vadose zone hydrology and implications for saprolite weathering, *Earth Surf. Processes Landforms*, 40(9), 1254–1269.
- LeBond, J. S., S. Strekopytov, C. Unsworth, B. J. Williamson (2011), Testing a new method for quantifying Si in silica-rich biomass using HF in a closed vessel microwave digestion system, *Anal. Methods*, 3, 1752–1758.

- Likens, G. E., et al. (1998), The biogeochemistry of calcium at Hubbard Brook, *Biogeochemistry*, *41*, 89–173.
- Lin, J., R. Ravella, B. Ketchum, P. R. Bierman, P. Heaney, T. White, and S. L. Brantley (2010), Mineral weathering and elemental transport during hillslope evolution at the Susquehanna/Shale Hills Critical Zone Observatory, *Geochim. Cosmochim. Acta*, *74*, 3669–3691.
- Liu, F., R. C. Bales, M. H. Conklin, and M. E. Conrad (2008a), Streamflow generation from snowmelt in semi-arid, seasonally snow-covered, forested catchments, Valles Caldera, New Mexico, *Water Resour. Res.*, *44*, W12443, doi:10.1029/2007WR006728.
- Liu, F., R. Parmenter, P. D. Brooks, M. H. Conklin, and R. C. Bales (2008b), Seasonal and Interannual variation of streamflow pathways and biogeochemical implications in semi-arid, forested catchments in Valles Caldera, New Mexico, *Ecohydrology*, *1*, 239–252.
- Louvat, P., and C. J. Allègre (1997), Present denudation rates on the island of Reunion determined by river geochemistry: Basalt weathering and mass budget between chemical and mechanical erosions, *Geochim. Cosmochim. Acta*, *61*(17), 3645–3669.
- Louvat, P., S. R. Gislason, C. J. Allègre (2008), Chemical and mechanical erosion rates in Iceland as deduced from river dissolved and solid material, *Am. J. Sci.*, *308*(5), 679–726.
- Lugolobi, F., A. C. Kurtz, and L. A. Derry (2010), Germanium–silicon fractionation in a tropical, granitic weathering environment, *Geochim. Cosmochim. Acta*, *74*(4), 1294–1308.
- Lybrand, R., C. Rasmussen, A. Jardine, P. Troch, and J. Chorover (2011), The effects of climate and landscape position on chemical denudation and mineral transformation in the Santa Catalina mountain critical zone observatory, *Appl. Geochem.*, *26*, S80–S84.
- Lyon, S. W., P. A. Troch, P. D. Broxton, N. P. Molotch, and P. D. Brooks (2008), Monitoring the timing of snowmelt and the initiation of streamflow using a distributed network of temperature/light sensors, *Ecohydrology*, *1*(3), 215–224.
- Maher, K. (2010), The dependence of chemical weathering rates on fluid residence times, *Earth Planet. Sc. Lett.*, *294*, 101–110.
- Maher, K. (2011), The role of fluid residence time and topographic scales in determining chemical fluxes from landscapes, *Earth Planet. Sc. Lett.*, *312*, 48–58.
- Maher K., and C. P. Chamberlain (2014), Hydrologic regulation of chemical weathering and the geologic carbon cycle, *Science*, *343*, 1502–1504.
- Maher, K., C. I. Steefel, A. F. White, and D. A. Stonestrom (2009), The role of reaction affinity and secondary minerals in regulating chemical weathering rates at the Santa Cruz Soil Chronosequence, California, *Geochim. Cosmochim. Acta*, *73*, 2804–2831.
- Manga, M. (2001), Using springs to study groundwater flow and active geologic processes, *Annu. Rev. Earth Planet. Sci.*, *29*(1), 201–228.
- McGuire, K. J., and J. J. McDonnell (2006), A review and evaluation of catchment transit time modeling, *J. Hydrol.*, *330*, 543–563.
- McIntosh, J., et al. (2017), Water chemistry for La Jara Creek and nearby springs in the Jemez River Basin Critical Zone Observatory, Valles Caldera Preserve, New Mexico (2010–2013), HydroShare. [Accessed from <https://doi.org/10.4211/hs.28639de860f74340a3549735abb7b0c6>].
- Miller, W. L., and R. G. Zepp (1995), Photochemical production of dissolved inorganic carbon from terrestrial organic matter: Significance to the oceanic organic carbon cycle, *Geophys. Res. Lett.*, *22*(4), 417–420.
- Molotch, N. P., P. D. Brooks, S. P. Burns, M. Litvak, R. K. Monson, J. R. McConnell, and K. Musselman (2009), Ecohydrological controls on snowmelt partitioning in mixed-conifer sub-alpine forests, *Ecohydrology*, *2*, 129–142.
- Moore, J., P. C. Lichtner, A. F. White, and S. L. Brantley (2012), Using a reactive transport model to elucidate differences between laboratory and field dissolution rates in regolith, *Geochim. Cosmochim. Acta*, *93*, 235–261.
- Moravec, B.G., et al. (2016), Coring the deep critical zone in the Jemez River Basin Critical Zone Observatory, Valles Caldera National Preserve, Northern New Mexico, Abstract EP41F-03 presented at 2016 Fall Meeting, AGU, San Francisco, Calif.
- Mortlock, R. A., and P. N. Froelich (1996), Determination of germanium by isotope dilution. Hydride generation inductively coupled plasma mass spectrometry, *Anal. Chim. Acta*, *332*, 277–284.
- Oades, J. M. (1988), The retention of organic matter in soils, *Biogeochemistry*, *5*(1), 35–70.
- Olyphant, J., J. D. Pelletier, and R. Johnson (2016), Topographic correlations with soil and regolith thickness from shallow-seismic refraction constraints across upland hillslopes in the Valles Caldera, New Mexico, *Earth Surf. Processes Landforms*, *41*(12), 1684–1696.
- Orem, C. A., and J. D. Pelletier (2016), The predominance of post-wildfire erosion in the long-term denudation of the Valles Caldera, New Mexico, *J. Geophys. Res. Earth Surface*, *121*, 843–864, doi:10.1002/2015JF003663.
- Pelletier, J. D., et al. (2013), Coevolution of nonlinear trends in vegetation, soils, and topography with elevation and slope aspect: A case study in the sky islands of southern Arizona, *J. Geophys. Res. Earth Surf.*, *118*, 741–758, doi:10.1002/jgrf.20046.
- Perdrial, J. N., N. Perdrial, A. Harpold, X. Gao, K. M. LaSharr and J. Chorover (2012), Impacts of sampling dissolved organic matter with passive capillary wicks versus aqueous soil extraction, *Soil Sci. Soc. Am. J.*, *76*, 2019–2030.
- Perdrial, J. N., et al. (2014a), Stream water carbon controls in seasonally snow-covered mountain catchments: Impact of inter-annual variability of water fluxes, catchment aspect and seasonal processes, *Biogeochemistry*, *118*(1–3), 273–290.
- Perdrial, J. N., N. Perdrial, A. Vázquez-Ortega, C. M. Porter, J. Leedy and J. Chorover (2014b), Experimental assessment of fiberglass passive capillary wick sampler (PCap) suitability for sampling inorganic soil solution constituents, *Soil Sci. Soc. Am. J.*, *78*, 486–495.
- Pokrovski, G. S., and J. Schoff (1998a), Experimental study of the complexation of silicon and germanium with aqueous organic species: Implications for germanium and silicon transport and Ge/Si ratio in natural waters, *Geochim. Cosmochim. Acta*, *62*, 3413–3428.
- Pokrovski, G. S., and J. Schott (1998b), Thermodynamic properties of aqueous Ge(IV) hydroxide complexes from 25 to 350°C: Implications for the behavior of germanium and the Ge/Si ratio in hydrothermal fluids, *Geochim. Cosmochim. Acta*, *62*, 1631–1642.
- Pokrovski, G. S., F. Martin, J. Hazeman, and J. Schott (2000), An X-ray absorption fine structure spectroscopy study of germanium-organic ligand complexes in aqueous solution, *Chem. Geol.*, *163*, 151–165.
- Probst, A., A. El Gh'mari, D. Aubert, B. Fritz, and R. McNutt (2000), Strontium as a tracer of weathering processes in a silicate catchment polluted by acid atmospheric inputs, Strengbach, France, *Chem. Geol.*, *170*(1), 203–219.
- Purtymun, W. D. (1967) Geology and physical properties of the near-surface rocks of Mesita de los Alamos, Los Alamos County, New Mexico, *U.S. Geol. Surv. Open-File Rep.*, *67–180*, 32 p.
- Rad, S., P. Louvat, C. Gorge, J. Gaillardet, C. J. Allègre (2006), River dissolved and solid loads in the Lesser Antilles: New insight into basalt weathering processes, *J. Geochem. Explor.*, *88*(1), 308–312.
- Rademacher, L. K., J. F. Clark, D. W. Clow, and G. B. Hudson (2005), Old groundwater influence on stream hydrochemistry and catchment response times in a small Sierra Nevada catchment: Sagehen Creek, California, *Water Resour. Res.*, *41*, W02004, doi:10.1029/2003WR002805.
- Rasmussen, C., and J. Chorover (2017), *Mixed Conifer Zero Order Basin Morphologic Horizon Geochemistry Data (New Mexico, USA), Integrated Earth Data Applications (IEDA)*, doi:10.1594/IEDA/100638.
- Rasmussen, C., S. M. Meding, A. Vasquez, and J. Chorover (2011), Domes, Ash and Dust: Controls on soil genesis in a montane catchment of the Valles Caldera, Abstract #EP51B-0845 presented at 2011 Fall Meeting, New Mexico, AGU, San Francisco, Calif.
- Rasmussen, C., J. D. Pelletier, P. A. Troch, T. L. Swetnam, and J. Chorover J. (2015), Quantifying topographic and vegetation effects on the transfer of energy and mass to the critical zone, *Vadose Zone J.*, *14*(11), doi:10.2136/vzj2014.07.0102.
- Reheis, M. C., J. R. Budahn, P. J. Lamothe (1999), Elemental analysis of modern dust in Southern Nevada and California, *U.S. Geol. Surv. Open File Rep.*, *99–53*.

- Reich, P. B., J. Oleksyn, J. Modrzyński, P. Mrozinski, S. E. Hobbie, D. M. Eissenstat, J. Chorover, O. A. Chadwick, C. M. Hale, and M. G. Tjoelker (2005), Linking litter calcium, earthworms and soil properties: A common garden test with 14 tree species, *Ecol. Lett.*, *8*, 811–818.
- Reneau, S. L., E. V. McDonald, J. N. Gardner, T. R. Kolbe, J. S. Carney, P. M. Watt, and P. A. Longmire (1996), Erosion and deposition on the Pajarito Plateau, New Mexico, and implications for geomorphic responses to late Quaternary climatic changes, in *The Jemez Mountains Region, Guidebook, 47th Field Conference*, edited by F. Goff et al., pp. 391–397, N. M. Geol. Soc.
- Schopka, H. H., L. A. Derry, and C. A. Arcilla (2011), Chemical weathering, river geochemistry and atmospheric carbon fluxes from volcanic and ultramafic regions on Luzon Island, the Philippines, *Geochim. Cosmochim. Acta*, *75*(4), 978–1002.
- Sebestyen, S. D., E. W. Boyer, J. B. Shanley, C. Kendall, D. H. Doctor, G. R. Aiken, and N. Ohte (2008), Sources, transformations, and hydrological processes that control stream nitrate and dissolved organic matter concentrations during snowmelt in an upland forest, *Water Resour. Res.*, *44*, W12410, doi:10.1029/2008WR006983.
- Shanley, J. B., W. H. McDowell, and R. F. Stallard (2011), Long-term patterns and short-term dynamics of stream solutes and suspended sediment in a rapidly weathering tropical watershed, *Water Resour. Res.*, *47*, W07515, doi:10.1029/2010WR009788.
- Sposito, G. (2008), *The Chemistry Of Soils*, Oxford Univ. Press, Oxford, U. K.
- Stallard, R. F., and S. F. Murphy (2014), A unified assessment of hydrologic and biogeochemical responses in research watersheds in eastern Puerto Rico using runoff–concentration relations, *Aquat. Geochem.*, *20*(2–3), 115–139.
- Steeffel, C. I., and K. Maher (2009), Fluid–rock interaction: A reactive transport approach, *Rev. Mineral. Geochem.*, *70*, 485–532.
- Thompson, R. S., C. Whitlock, P. J. Bartlein, S. P. Harrison, and W. G. Spaulding (1993), Climatic changes in the western United States since 18,000 yr B.P., in *Global Climates Since the Last Glacial Maximum*, edited by H. E. Wright Jr., et al., pp. 468–515, Univ. of Minn. Press, Minneapolis, Minn.
- Trostle, K. D., J. Ray Runyon, M. A. Pohlmann, S. E. Redfield, J. Pelletier, J. McIntosh, and J. Chorover (2016), Colloids and organic matter complexation control trace metal concentration–discharge relationships in Marshall Gulch stream waters, *Water Resour. Res.*, *52*, 7931–3944, doi:10.1002/2016WR019072.
- Uchida, T., Y. Asano, N. Ohte, and T. Mizuyama (2003), Seepage area and rate of bedrock groundwater discharge at a granitic unchanneled hillslope, *Water Resour. Res.*, *39*(1), 1018, doi:10.1029/2002WR001298.
- Vázquez-Ortega, A., et al. (2015), Rare earth elements as reactive tracers of biogeochemical weathering in forested rhyolitic terrain, *Chem. Geol.*, *391*, 19–32.
- Vázquez-Ortega, A., D. Huckle, J. Perdrial, M. K. Amistadi, M. Durcik, C. Rasmussen, J. McIntosh, and J. Chorover (2016), Solid-phase redistribution of rare earth elements in hillslope pedons subjected to different hydrologic fluxes, *Chem. Geol.*, *426*, 1–18.
- Vuataz, F. D., and F. Goff (1986), Isotope geochemistry of thermal and nonthermal waters in the Valles Caldera, Jemez Mountains, northern New Mexico, *J. Geophys. Res.*, *91*(B2), 1835–1853.
- Weng, C., and S. T. Jackson (1999), Late Glacial and Holocene vegetation history and paleoclimate of the Kaibab Plateau, Arizona, *Palaeogeogr. Palaeoclimatol. Palaeoecol.*, *153*, 179–201.
- White, A. F., A. E. Blum, M. S. Schulz, D. V. Vivit, D. A. Stonestrom, M. Larsen, M., S. F. Murphy, and D. Eberl (1998), Chemical weathering in a tropical watershed, Luquillo Mountains, Puerto Rico: I. Long-term versus short-term weathering fluxes, *Geochim. Cosmochim. Acta*, *62*(2), 209–226.
- White, A. F., A. E. Blum, D. A. Stonestrom, T. D. Bullen, M. S. Schulz, T. G. Huntington, and N. E. Peters (2001), Differential rates of feldspar weathering in granitic regoliths, *Geochim. Cosmochim. Acta*, *65*, 847–869.
- White, A. F., M. S. Schulz, D. V. Vivit, A. E. Blum, D. A. Stonestrom, and S. P. Anderson (2008), Chemical weathering of a marine terrace chronosequence, Santa Cruz, California I: Interpreting rates and controls based on soil concentration–depth profiles, *Geochim. Cosmochim. Acta*, *72*, 36–68.
- White, A. F., M. S. Schulz, D. A. Stonestrom, D. V. Vivit, J. Fitzpatrick, T. D. Bullen, K. Maher, A. E. Blum (2009), Chemical weathering of a marine terrace chronosequence, Santa Cruz, California. Part II: Solute profiles, gradients and comparisons of contemporary and long-term weathering rates, *Geochim. Cosmochim. Acta*, *73*, 2769–2803.
- Williams, M. W., and J. M. Melack (1991), Solute chemistry of snowmelt and runoff in an alpine basin, Sierra Nevada, *Water Resour. Res.*, *27*(7), 1575–1588.
- Zapata-Rios, X., P. D. Brooks, P. A. Troch, J. McIntosh, and Q. Guo (2015a), Influence of terrain aspect on water partitioning, vegetation structure and vegetation greening in high-elevation catchments in northern New Mexico, *Ecohydrology*, *9*, 782–795, doi:10.1002/eco.1674.
- Zapata-Rios, X., J. McIntosh, L. Rademacher, P. A. Troch, P. D. Brooks, C. Rasmussen, and J. Chorover (2015b), Climatic and landscape controls on water transit times and silicate mineral weathering in the critical zone, *Water Resour. Res.*, *51*, 6036–6051, doi:10.1002/2015WR017018.